İSTANBUL TECHNICAL UNIVERSITY ★ INSTITUTE OF SCIENCE AND TECHNOLOGY

THE EFFECT OF HYDRATION ON CAPILLARY POROSITY AND CONCRETE PERMEABILITY

M.Sc. Thesis by

Hüseyin Oytun YAZAN, B.Sc.

501051143

Date of submission : 7 May 2007

Date of defence examination: 12 June 2007

Supervisor (Chairman): Assoc. Prof. Dr. Yılmaz AKKAYA

Members of the Examining Committee Prof.Dr. Mehmet Ali TAŞDEMİR

Prof.Dr. Fevziye AKÖZ (Y.T.Ü.)

JUNE 2007

İSTANBUL TEKNİK ÜNİVERSİTESİ ★ FEN BİLİMLERİ ENSTİTÜSÜ

HİDRATASYONUN KAPİLER BOŞLUK SİSTEMİNE VE BETON GEÇİRİMLİLİĞİNE ETKİSİ

YÜKSEK LİSANS TEZİ

Müh. Hüseyin Oytun YAZAN

(501051143)

Tezin Enstitüye Verildiği Tarih : 7 Mayıs 2007

Tezin Savunulduğu Tarih : 12 Haziran 2007

Tez Danışmanı : Doç.Dr. Yılmaz AKKAYA

Diğer Jüri Üyeleri Prof.Dr. Mehmet Ali TAŞDEMİR

Prof.Dr. Fevziye AKÖZ (Y.T.Ü.)

HAZİRAN 2007

ACKNOWLEDGEMENTS

I would like to express my sincere appreciation to my supervisor Dr.Yılmaz Akkaya, who gave me the chance to work in the Marmaray Laboratory in the Civil Engineering Faculty at ITU and offered me the valuable guidance, inspiring discussions and continous support throughout the whole period of two years, not only in the research process of this thesis but also at the works of the project of Marmaray Bosphorus Crossing 1.

I am also grateful to my lecturer and the Dean of the Civil Engineering Faculty Prof. Mehmet Ali Taşdemir. I would like to thank Prof. Taşdemir for his valuable comments and his continous supports. I am deeply moved by his fascinating involvement in scientific research and international science cooperation.

I would like to thank my colleague and dear friend Tahsin Alper Yıkıcı, who acquired the thin section images and shared his valuable opinions and engineering experiences with me during the hard work of the Marmaray Laboratory and my thesis and who also motivated me to my thesis with his great sense of humor.

Marmaray Project contractor GamaNurol's ITU representative Neşe Şahin is greatfully acknowledged, because of her effort for supplying materials for the experimental phase of this work.

My special thanks go to the technicians of the Marmaray Laboratory, namely, Mehmet Ali Küçük, Namık Kemal Özkan, Cüneyt Yıldız and Erdoğan Kılavuz, who gave me great support and shared creative ideas by the experimental procedure of my thesis.

I would like to extend my deep appreciation to Tuğçe Katipoğlu, for her powerful support and close interest during the writing of this thesis.

Last but not least, I wish to thank my family for their encouragement and support throughout my study and my life.

İstanbul, May 2007 Hüseyin Oytun Yazan

TABLE OF CONTENTS

ABBREVIATIONS

ITZ	: Interfacial Transition Zone
C_3S	: Tricalcium Silicate
C_2S	: Dicalcium Silicate
C_3A	: Tricalcium Aluminate
C_4AF	: Ferrit phase
CSH	: Calcium Silicate Hydrate
CH	: Calcium Hydroxide
HCP	: Hardened Cement Paste
MIP	: Mercury Intrusion Porosimetry
AVA	: Air Void Analysis

LIST OF TABLES

LIST OF FIGURES

LIST OF SYMBOLS

α	: Degree of hydration
A	: Capillary coefficient
β	: Turtuosity
c	: Chloride concentration
c_f	: Free chloride concentration
c_s	: Surface chloride concentration
D	: Diffusion coefficient
D_a	: Apparent diffusion coefficient
E	: Electrical potential
E(θ)	: Activation energy
erf	: Error function
F	: Faraday number
F_w	: Flux of water
H	: Velocity function
k	: Water permeability
λ	: Mean free spacing
l_c	: Critical pore diameter
M	: Maturity
φ	: Electrical conductivity
p	: Porosity
ρ	: Density
Q_{cl}	: Amount of chlorides
R	: Gas constant
θ	: Temperature
T	: Absolute temperature
t	: Time
V	: Volume
w/c	: Water to cement ratio
X	: Gel to space ratio

HİDRATSYONUN KAPİLER BOŞLUK SİSTEMİNE VE BETON GEÇİRİMLİLİĞİNE ETKİSİ

ÖZET

Bu çalışmada, hidratasyon, boşluk yapısı ve klor geçirimlilik süreçleri gibi betonun mikro yapısını ilgilendiren kavramlar için literatür taranmış, boşluk yapısı ve beton geçirimliliğiyle ilgili deneyler ayrıntılı biçimde sunulmuştur.

Yapılan deneysel çalışmalarda, literatür çalışmasında gösterilmiş bazı deneyler sertleşmekte olan ve sertleşmiş beton numuneler üzerinde uygulanmıştır. Özellikle ışık yoğunluğu analizi adı verilen yeni bir deney metodu ile sertleşmekte olan betonlardan üretilmiş ince kesitler üzerinde kapiler porozitenin gelişimi hidratasyon süresince incelenmiştir.

Deneysel çalışmalarda ayrıca, uçucu küllü ve mikrosilikalı ve mineral katkısız olmak üzere çimento hamurları dökülmüş ve bu hamurların hidratasyon derecesi gelişimi incelenmiştir. Hidratasyon derecesine bağlı olarak, boşlukta jel oranları hesaplanmıştır. Buna ek olarak, uçucu küllü ve mikrosilikalı ve mineral katkısız beton numuneleri dökülmüştür. Bu numuneler sertleşme sürecinde ve sertleşme sonrasında teste tabi tutulmuşlardır.

Değişen su/çimento oranlarında, kapiler boşluk hacmi ve hidratasyon arasındaki ilişkiyi kurabilmek için adyabatik ısı gelişimi ve ışık yoğunluğu deneyleri sertleşmekte olan betonlara uygulanmıştır. Su/çimento oranı arttıkça kapiler boşluk hacminin arttığı, mukavemetin düştüğü ve ışık yoğunluğunun hidratasyon boyunca azaldığı görülmüştür.

Hızlı klor geçirimliliği deneyleriyle mineral katkıların geçirimliliği azaltıcı etkisi görülmüştür. Sertleşmiş numunelere kapiler su emme deneyi uygulanarak su emme oranlarının zamanla nasıl değiştiği gösterilmiştir.

Ayrıca sertleşmiş numunelere hava boşluğu analizi yapılarak numunelerde su/çimento oranın artmasıyla toplam hava içeriğinin arttığı saptanmıştır.

THE EFFECT OF HYDRATION ON CAPILLARY POROSITY AND CONCRETE PERMEABILITY

SUMMARY

In this document, a literature review of concrete microstructure properties, such as hydration, pore structure and chloride transport processes are made. The test methods for determination of pore structure and concrete permeability are also presented in detail.

In the experimental phase, some of the test methods were applied to hardening concrete and hardened concrete samples, which were mentioned in the literature review. Especially a new test method, namely, the light intensity analysis were executed on thin sections of hardening concrete samples to state the development of capillary porosity during hydration.

In this study cement pastes are cast with and without mineral additives, namely, fly ash and microsilica, and their hydration degree development is investigated. According to the hydration degree results, gel to space ratio values are computed. In addition to this, concrete samples were cast with and without mineral additives and tested during the hardening process and after they have hardened.

Adiabatic heat development and light intensity analysis are performed on hardening samples to indicate the relationship between hydration and capillary pore volume by varying water to cement ratios. As the water to cement ratio increases the capillary pore volume increases, the compressive strength decreases and the light intensity decreases during hydration.

Rapid chloride permeability test on hardened samples the permeability reducing effect of mineral additives and capillary water absorption test showed the variance of the absorption rates in time.

Additionally, air void analysis of hardened samples has indicated that the total air content increase with an increase of water to cement ratio.

1. INTRODUCTION

1.1 Background

Ancient Egyptians and the Romans used concrete to build spectacular structures in order to exhibit the magnificance of their civilizations. Those structures still remain after thousands of years. Concrete has proven itself to be the most durable construction material ever throughout the history.

Durability is the ability of concrete to resist weathering action, chemical attack, and abrasion while maintaining its desired engineering properties **(PCA,2007)**. Durability concept was percieved by many civil engineers recently, because of high level of maintanence expenses for a wide range of structures, especially for concrete bridges, pavements and water structures. A structure is considered durable if it exhibits the required working properties with low maintanence cost and resists the subjected aggressive exposures from environment throughout the project service life.

1.2 Objectives and scope

In this document, a literature review of concrete microstructure properties, such as hydration, pore structure and chloride transport processes are made. The test methods for determination of pore structure and concrete permeability are also presented in detail.

In the experimental phase, some of the test methods were applied to hardening concrete and hardened concrete samples, which were mentioned in the literature review. Especially a new test method, namely, the light intensity analysis were executed on thin sections of hardening concrete samples to state the development of capillary porosity during hydration.

2. CONCRETE MICROSTRUCTURE

Concrete is an extremely complex system structured of solid phases, pores and water with high degree of heterogenity. Microstructural features depend on many factors, such as the physical and chemical nature of the cement and aggregates, the amount of admixture added to it, temperature, hydration period, the initial w/c ratio, porosity, pore shape, and pore size distribution. Concrete is a particulate composite material, revealing size segregation of particles on different scales from boundary effects near the formwork to interfacial transition zones (ITZs) around aggregate grains **(Hu, 2004)**.

2.1 Hydration

2.1.1 Composition of Portland cement

Tricalcium silicate ($3CaO•SiO_2$), dicalcium silicate ($2CaO•SiO_2$), tricalcium aluminate ($3CaO•Al_2O_3$), and a ferrite phase of $4CaO•Al_2O_3•Fe_2O_3$ are the main components of portland cement. $3CaO•SiO_2$ phase is a solid solution containing Mg and Al and is called alite. The $2CaO•SiO_2$ phase, called belite, contains K_2O in addition to Al and Mg. The ferrite phase, shown as C_4AF, is a solid solution of variable composition from C_2F to C_6A_2F. Potential components of this compound are C_2F, C_6AF_2, C_4AF, and C_6A_2F **(Ramachandran et al., 2001)**.

2.1.2 Hydration mechanism

Tricalcium silicate (C_3S) and dicalcium silicate (C_2S) constitute approximately 75% by mass of dry cement. When cement is mixed in water chemical reactions take place that result in the formation of hydration products. The two silicate phases give calcium-silicate-hydrate (CSH) and calciumhydroxide (CH) as hydration products, which constitute approximately 50-60% and 20-25% of the total volume of the hydrated product respectively. Hardened cement paste contains CSH gel, crystals of calciumhydroxide, ettringite and minor residues of the original unhydrated cement and residues of the original water-filled spaces in the fresh paste.

At the first step, when C_3S comes into contact with water there is a rapid evolution of heat and this ends approximately within 20 minutes, where calcium and hydroxyl ions were released into the solution. This stage is called the preinduction period. In the induction period, the reaction rate is very slow and may extend for a few hours.

At this second stage, the dissolution continues and pH reaches a high value of 12.5. Not much silica dissolution occurs at this stage and the cement remains plastic and is workable. In the third stage, after a certain critical value of calcium and hydroxide ions is reached, there is a rapid crystallization of calciumhydroxide (CH) and calcium-silicate-hydrate (CSH) followed by a rapid reaction, which occurs actively and accelerates with time, reaching a maximum rate at the end of this accelerating period. Initial stiffening occurs at about the time when the rate of reaction becomes vigorous. The final set occurs before the end of the third stage. In the fourth stage, there is slow deceleration. There is a continuous formation of hydration products. Finally, there is only a slow formation of products and at this stage the reaction is diffusion controlled **(Ramachandran et al., 2001)**.

2.1.3 Hydration behaviour of individual cement compounds

C_3S and C_2S together make up approximately 75% of portland cement. In the presence of a limited amount of water, the reaction of C_3S with water can be shown as follows:

$$2[3CaO{\bullet}SiO_2] + 7H_2O \rightarrow 3CaO{\bullet}2SiO_2{\bullet}4H_2O + 3Ca(OH)_2 \qquad \textbf{(2.1)}$$

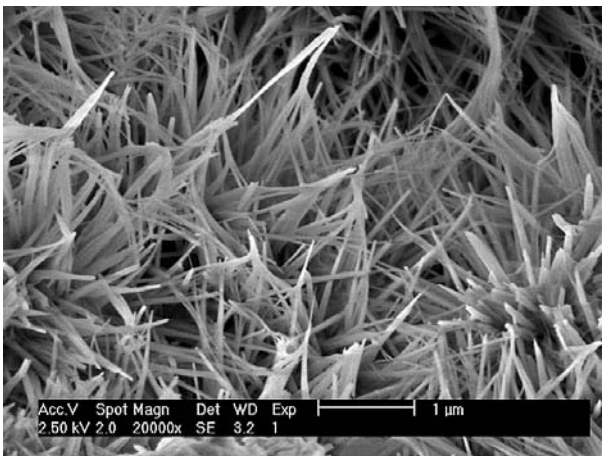

Figure 2.1 : Fibrous CSH phases by the hydration of C_3S **(Stark et al., 2001)**.

The hydration of C_2S phase proceeds in a similar way to that of C_3S, but is much slower. The hydration of C_2S can be represented by the equation.

$$2\,[2CaO{\bullet}SiO_2] + 5H_2O \rightarrow 3CaO{\bullet}2SiO_2{\bullet}4H_2O + Ca(OH)_2 \qquad \textbf{(2.2)}$$

The amount of $Ca(OH)_2$ formed in this reaction is less than that produced in the hydration of C_3S.

Although the average tricalcium aluminate (C_3A) content in portland cement is about 4–11%, it significantly influences the early reactions. The phenomenon of flash set, the formation of various calcium aluminate hydrates and calcium carbo- and sulfo-aluminates, involves the reactions of C_3A. Tricalcium aluminate reacts with water to form C_2AH_8 and C_4AH_{13}. These products are thermodynamically unstable so that without stabilizers or admixtures they convert to the C_3AH_6. The relevant equations for these reactions are:

$$2C_3A + 21H \rightarrow C_4AH_{13} + C_2AH_8 \quad \textbf{(2.3)}$$

$$C_4AH_{13} + C_2AH_8 \rightarrow 2C_3AH_6 + 9H \quad \textbf{(2.4)}$$

Table 2.1: The main components in the hydrated Portland cement paste **(Yang, 2006)**

Main Components	Chemical compositon	Morphologies	
CSH gel	$CaO\text{-}SiO_2\cdot nH_2O$	outer product gel	prominent at early stages of hydration, more open, structured and porous morphologies: • Type I: fibrous, up to 2 μm in length, <0.2 μm across; • Type II: honeycomb or reticular
		inner product gel	prominent in older pastes: • Types III, more massive and appears to consist of tightly packed equant grains up to 300 nm across; • Type IV, still more featureless and massive.
Calcium Hydroxide	$(CaOH)_2$ portlandite	Ideal conditions: hexagonal crystal with good cleavage; In cement paste: layer structure, massive and of indeterminate shape	
Calcium Aluminoferrite Hydrate	$[Ca_2(Al,Fe)(OH)_6]_2\cdot X\cdot nH_2O$	thin hexagonal platelets	
Calcium Aluminoferrite Hydrate	$[Ca_3(Al,Fe)(OH)_6\cdot 12H_2O]_2\cdot X\cdot nH_2O$ ettringite	prismatic or acicular, slender needles	
Calcium Sulfate Hydrate	$CaSO_4\cdot nH_2O$	Tablets or prisms	

In portland cement, the hydration of the C_3A is controlled by the addition of gypsum. The flash set is thus avoided. The C_3A phase reacts with gypsum in a few minutes to form ettringite as follows:

$$C_3A + 3CSH_2 + 26H \rightarrow C_3A\bullet 3CSH_{32} \quad \textbf{(2.5)}$$

After all gypsum is converted to ettringite, the excess C_3A will react with ettringite to form the low sulfo-aluminate hydrate.

$$C_3A\bullet 3CSH_{32} + 2C_3A + 4H \rightarrow 3[C_3A\bullet CSH_{12}] \quad \textbf{(2.6)}$$

Gypsum is a more effective retarder than lime for C_3A hydration and together they are even more effective than either of them.

The C_4AF phase is known to yield the same sequence of products as C_3A, however, the reactions are slower **(Ramachandran et al., 2001)**. In the presence of water, C_4AF reacts as follows:

$$C_4AF + 16H \rightarrow 2C_2(A,F)H_8 \quad \textbf{(2.7)}$$

$$C_4AF + 16H \rightarrow C_4(A,F)H_{13} + (A,F)H_3 \quad \textbf{(2.8)}$$

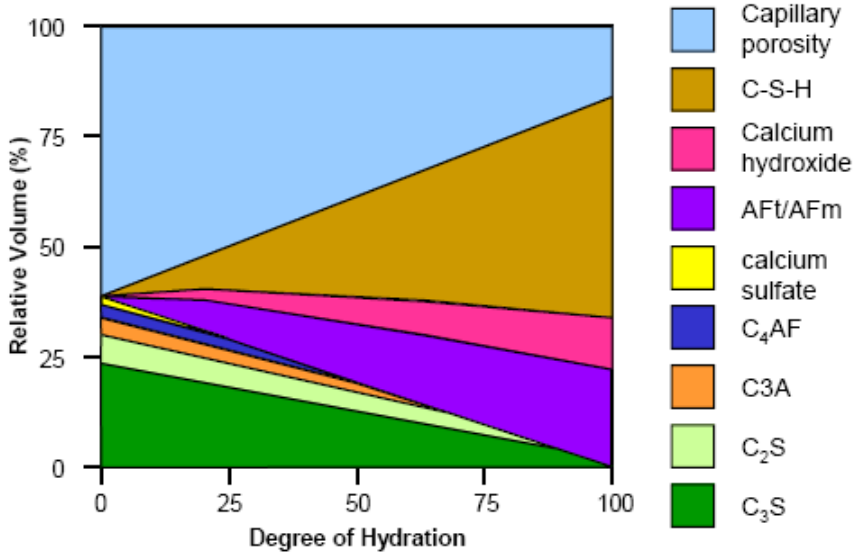

Figure 2.2 : Relative volume development in cement paste depending on degree of hydration **(Kurtis, 2007)**.

2.1.4 Adiabatic heat development

This test method determines the amount of heat developed in concrete during the hydration process. The heat development is described in terms of the produced energy as a function of the maturity of the concrete **(NT BUILD 388, 1992)**.

The maturity method has been developed to predict the in-place compressive strength development of concrete based on its thermal history. The maturity function can be expressed as

$$M = \sum_{i=1}^{n} H(\theta_i) \cdot \Delta t_i \qquad \textbf{(2.9)}$$

where M is the maturity, Δt_i the length of time interval i, θ_i the mean temperature in time interval i and $H(\theta_i)$ the velocity function, which can be stated as

$$H(\theta) = \exp[\frac{E(\theta)}{R} \cdot (\frac{1}{293} - \frac{1}{273+\theta})] \qquad \textbf{(2.10)}$$

where R is the gas constant, 8.314 J/mol·K and $E(\theta)$ the activation energy for the concrete mix. If the correct value of $E(\theta)$ is unknown the following can be used:

$$\begin{aligned} E(\theta) &= 33500 && \text{J/mol for } \theta \geq 20°\text{C} \\ E(\theta) &= 33500 + 1470 \cdot (20 - \theta) && \text{J/mol for } \theta < 20°\text{C} \end{aligned} \qquad \textbf{(2.11)}$$

As stated in the experimental work phase, this test method was used in order to determine the hydration development of concrete.

2.2 Pore structure

The rate of transport of water is influenced by the microstructure of concrete, for example, by the amount of pores, the pore size distribution, and the interconnection of pores and also by the location, frequency and interconnection of cracks and other defects. The sizes of pores in the cement paste embraces several orders of magnitude. According to the origin and characteristics the pores are described as compaction pores (entrapped air), air voids (entrained air), capillary pores, and gel pores.

There is no sharp size variation between capillary and gel pores. The capillary pores are considered to have a size ranging from hundreds of micrometers down to tens of nanometers, with the upper end of the CSH gel pore size distribution overlapping the lower end of the capillary pore size range **(Mindess et al., 1981)**.

Pore structure is significantly affected by the hydration of cement. Cement hydration is the function of chemical composition of cement, cement grading, cement fineness, water to cement ratio and temperature. Therefore degree of hydration is an important scale for the development of porosity and pore size distribution. Since hydration products fill the available space in the paste gradually, the total porosity decreases during the process. **(Hu, 2004)**.

The capillary pore space, the water-filled space between the cement particles and their reaction products that is left over from the original cement-water mixture. There are nanometer-scale pores in the CSH surface product material, which form continuous pathways, called gel pores. However, transport properties are dominated by the much larger capillary pores as long as they percolate, i.e., form a continuous pathway.

Concrete porosity is the interconnectivity of pores. A concrete with a high proportion of disconnected pores may be less permeable that a concrete with a much smaller proportion of connected, or continuous pores. **Halamickova et al. (1995)** stated that the pore structure of the cement paste has to be considered especially in their size and connectivity. The nature of the matrix pore structure affects permeability significantly. The size, distribution, interconnectivity, shape, and tortuosity of pores are all determining factors in the overall permeability of a concrete matrix.

2.2.1 Microstructure of hardened cement paste

The actual microstructure of hardened cement paste (hcp) is unknown yet, because of the amorphous structure of CSH with varying chemical composition. A few models have been suggested to describe the structure of hcp, namely, Powers, Feldman and Sereda and Munich **(Mindess et al., 1981)**.

Powers' model describes gel as a rigid substance made up of colloidal size particles and with a characteristic porosity of 28%, which is due to the presence of gel pores. In addition to the gel pores, capillary pores are the remains of the original water-filled space. These two type pores contribute the porosity of hcp. Water in the hardened cement paste is classified as non-evapourable (chemically bound) and evapourable (can be removed at 105°C). Non-evapourable water particles are represented as "x" in **Figure 2.3** and in **Figure 2.4** in interlayer sheets, which are represented as lines. Evapourable water particles are designated as "o", which are

adsorbed on surfaces and capillary pores as “C”. Quantitative calculations of the volumetric composition of hcp are mainly based on this model **(Powers et al., 1948)**.

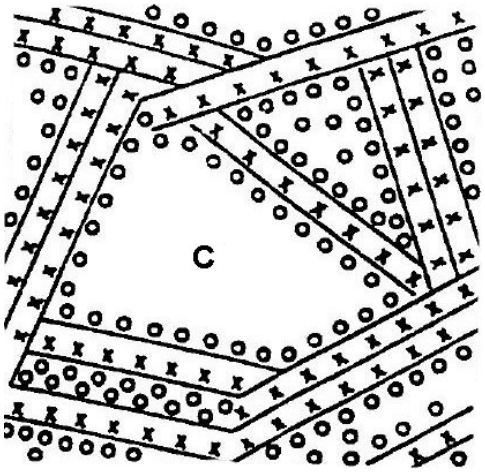

Figure 2.3 : Powers Model **(Mindess et al., 1981)**.

Powers also stated the volume fractions of unhydrated cement, capillary pores and gel pores. As shown below the formulas are:

$$V_{unhydrated\ \ cement} = \frac{0.32(1-\alpha)}{w_0/c + 0.32} \tag{2.12}$$

$$V_{gel} = \frac{0.68\alpha}{w_0/c + 0.32} \tag{2.13}$$

$$V_{capillary\ \ pores} = \frac{w_0/c - 0.36\alpha}{w_0/c + 0.32} \tag{2.14}$$

where α is the degree of hydration of the cement, w_0/c is the initial water to cement ratio, and 0.32 cm^3/g is the average specific volume of portland cement.

In addition to above formulas Powers proposed another concept, namely, gel to space ratio in order to estimate the mechanical properties of cement concrete.

$$X_C = \frac{0.68\alpha}{0.32\alpha + w_0/c} \tag{2.15}$$

where X_C is the gel to space ratio, α is the hydration degree of cement and w_0/c is the water to cement ratio.

Feldman and Sereda’s model consists of irregularly arranged single layer sheets with a thickness of 2-4 water molecules. In this model, the water in hcp is classified as interlayer hydrate water and physically adsorbed water **(Feldman et al., 1968)**.

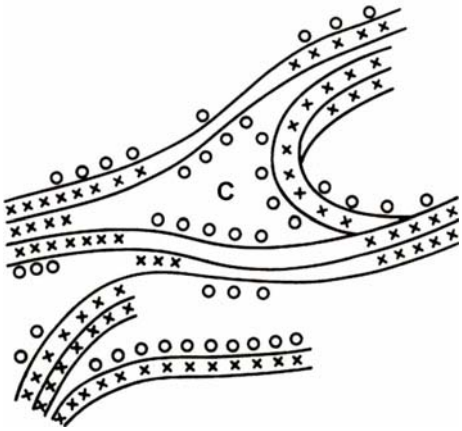

Figure 2.4 : Feldman-Sereda Model **(Mindess et al., 1981)**.

The Munich model considers CSH as a three-dimensional network of colloidal size particles (xerogel). In this model, the water is not classified specifically, except that water is strongly attracted to solid surfaces as adsorbed water, where solid surfaces are represented as rectangles with parallel lines **(Mindess et al., 1981)**.

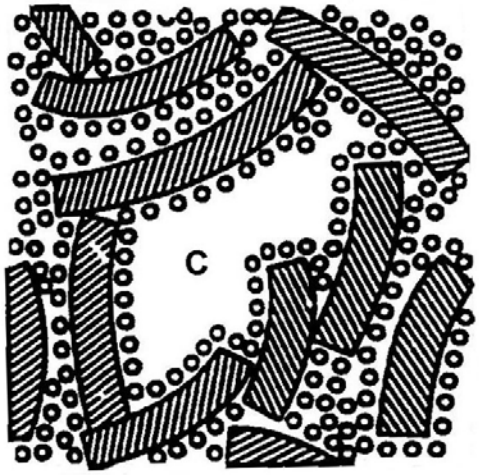

Figure 2.5 : Munich Model **(Mindess et al., 1981)**.

2.2.2 Permeability

Permeability of concrete may be defined as the property which characterizes the ease with which a fluid passes into and through the body of the concrete under a pressure differential. Although the term permeability is strictly related to a flow that occurs under a pressure differential, it is used most frequently to include other transport mechanisms such as absorption and diffusion. Permeability is mistaken for porosity and vice versa. It is conceivable, though improbable, that a concrete could be porous,

but impermeable if it contained a series of disconnected air pockets separated by impermeable material **(Ramachandran et al., 2001)**.

2.2.2.1 ITZ

ITZ is a thin layer of cement paste in contact with the aggregate particles, with higher porosity, conductivity and water to cement (w/c) ratio than the surrounding bulk paste **(Jaiswal et al., 1998)**.

An approximate extent of 15 μm in width around each aggregate grain is formed because of the so called "wall" effect during cement hydration, where less cement grains are present in the fresh state. But ITZ is not a definite zone, it is a region of transition **(Scrivener et al., 2004)**. In the fresh state of particle packing, the wall-effect causes of a reduction in the cement particle density, which implies a more porous zone than the bulk paste. As a result of size segregation, small particles tend to agglomerate in the vicinity of the aggregate surface, where the w/c ratio is much higher than in bulk paste **(Hu and Stroeven, 2004)**.

According to **Bentz and Garboczi (1999)** ITZ thickness equals to the median size of the cement particles and the ITZ thickness is not related to the w/c ratio. However, w/c ratio influences ITZ thickness. At lower w/c ratios the ITZ thickness will be reduced **(Hu and Stroeven, 2004)**. **Zimbelmann (1985)** and **Scrivener (1999)** also demonstrated experimentally that lower w/c ratio reduce the ITZ thickness and contribute to the interfacial bond strength.

ITZ affects the strength of concrete significantly, where concrete shows its quasi-ductile behaviour, because a decrease of load bearing capacity is obtained after the peak load. Such response of concrete to compression is a result of multiple microcracking observed in the ITZ **(Scrivener et al., 2004)**.

2.2.2.2 Tortuosity

As the volume fraction of aggregate increases, the paths that the transport fluid follow through the material become longer and more twisted in order to pass around the aggregates. This phenomenon is called tortuosity. tortuosity effects would appear as a reduction in permeability below that expected from dilution alone. The rate of increase in tortuosity is larger at low aggregate volume fractions as compared with higher volume fractions. Thus, the combination of dilution and tortuosity would induce a decreasing effect of permeability as the volume fraction of aggregate increases **(Jaiswal et al., 1998)**.

2.2.2.3 Dilution

Concretes with high volume fractions of aggregate would have less cement available in which transport could take place. This mechanism would induce a linear dependence of permeability on the volume fraction of aggregate **(Jaiswal et al., 1998)**.

2.2.2.4 Sorption

The dictionary explanation of sorption is the effect of gases or liquids being incorporated into a material of a different state and adhering to the surface of another molecule. Sorption appears mostly in cement based materials, where capillary suction forces attract water molecules and absorb them into the material.

2.2.3 Transport models

Methods used for the determination of water permeability of cement paste and concrete are very time-consuming. Therefore, some models have been used to depict the continous change of cement paste permeability.

2.2.3.1 Katz-Thompson

Katz and Thompson used percolation concepts to derive an equation relating the permeability of saturated random porous media to microstructural descriptors and conductivities. As **Hu (2004)** stated, the equation was directly applied in order to predict the water permeability k of ordinary Portland cement:

$$k = \frac{1}{226} l_c^{\,2} \frac{\vartheta}{\vartheta_0} \qquad \textbf{(2.16)}$$

where l_c is the critical pore diameter, ϑ is the electrical conductivity of the sample and ϑ_0 is the electrical conductivity of the pore solution. The ratio of the solution conductivity to sample conductivity is called formation factor.

2.2.3.2 Carmen-Kozeny

According to this model the water permeability k of cement paste can be estimated on the morphological basis of the pore space by

$$k = -\frac{p(V_{pore} / S_{pore})^2}{2\beta} \qquad \textbf{(2.17)}$$

where p is porosity, V_{pore} and S_{pore} are the volume and surface area of the pore space and β is the tortuosity in the cement paste. Permeability is proportional to the second power of $V_{pore} / S_{pore} = \lambda / 4$ where λ is mean free spacing between solid phases, which are reflecting the average pore size **(Hu, 2004)**.

2.3 Chloride transport processes

Chloride ingress into concrete structures in varying conditions may cause important damages and affect the durability and service life of structures, because chlorides initiate corrosion of the reinforcement. When corrosion effects start to increase, corrosion products may have increased in volume and they can cause the spalling of the concrete cover and strength and serviceability properties reduce significantly. This problem leads engineers to apply early repair or cast repair concrete at the deteriorated surface.

It is also denotable, that a certain amount of chloride must be present near the steel surface before chloride causes corrosion. This amount of chloride is called as chloride threshold level, which is not a single value valid for all concretes **(Nilsson et al., 1996)**.

Chloride penetration is the outcome of several chloride transport and binding processes, which can be presented as chloride profile charts, where the distribution of chlorides with depth from the concrete surface for different exposure periods is shown.

The distribution of chlorides is a function of time, where enviromental effects, such as the chemical composition, concentration of solutions exposed to the concrete, and the material properties play a great role in the process. Especially in marine structures at the splash zone above sea water level, salt water is absorbed into concrete. At the same level rain water may remove some chlorides.

Water penetration depends on the magnitude of the flow, which is the result of permeability, the pressure gradient and the evaporation possibility **(Nilsson et al., 1996)**.

2.3.1 Chloride binding

Chloride binding process is crucial for concrete, because chloride ions in the pore solution are removed to the hydrated binder phase. The binding process reduces the

concentration in the solution for transportation. Only the dissolved ions harm reinforcement. Therefore the chloride binding capacity of concrete is an important issue itself.

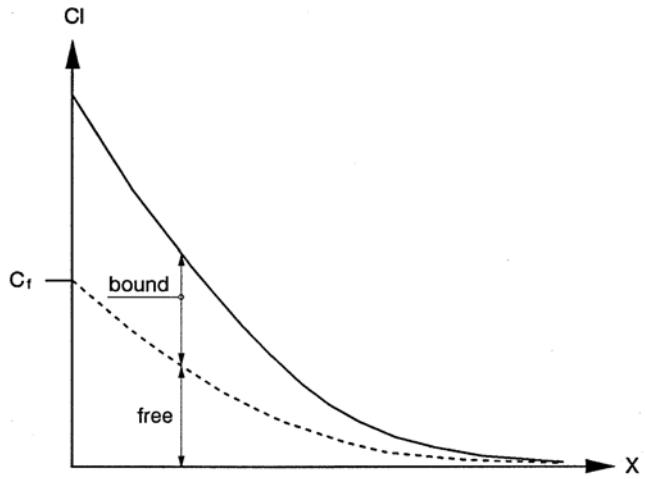

Figure 2.6 : Typical profiles for free and bound chlorides **(Nilsson et al., 1996)**.

Chlorides affect the microstructure of concrete by altering the hydration process and the pore size distribution of the hydrated binder.

The amount of bound chlorides depends on chloride concentration, fineness and content of the binder, water-cement ratio, degree of hydration, temperature, pH etc. High temperatures dissolve chlorides in the solution and decrease the amount of bound chlorides and fly ash and cement with high C_3A content bind more chlorides. It is noticable that Friedel's salt is the major binding product ($C_3A{\cdot}CaCl_2{\cdot}10H_2O$). Silica fume has a complex effect on the issue, such that CSH content is increased, secondly, silica reaction consumes alkalis and reduces pH, which increase the binding capacity. On the other hand the C_3A content decreases when the cement is replaced with the silica fume, which leads to a reduction in binding **(Nilsson et al., 1996)**.

2.3.2 Chloride diffusion

Pure diffusion of ions is the result concentration difference, which is formulated by Fick as the concentration gradient of ions:

$$F = -D\frac{\partial c}{\partial x} \qquad \textbf{(2.18)}$$

where F is the flux of ions in [kg/m^{2}s] and D is the diffusion coefficient in [m^2/s]. It is assumed that the system is steady state and the negative sign stands for the balance of the negative gradient of concentration.

In diffusion, the movement of negative ions must be balanced with positive ions, but Cl^- and Na^+ diffuse differently, so other ions like OH^- and Ca^{2+} may join the diffusion process when a salt solution is exposed to the surface of concrete.

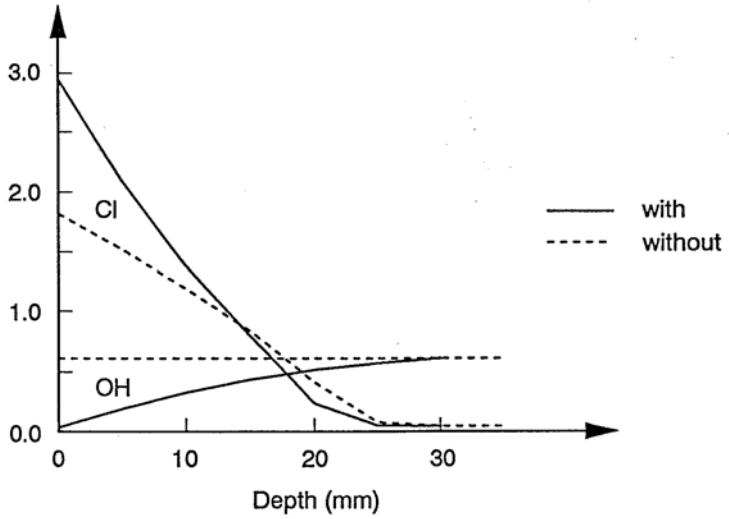

Figure 2.7 : The effect of leaching of alkalis **(Nilsson et al., 1996)**.

Leaching of hydroxides and alkalis is another point in the process. The absence of these molecules near surface regions cause a drop of pH and total content of chlorides increase, because of the increase of chloride binding capacity. Further leaching of hydroxides cause deterioration of CSH gel, which decreases the binding capacity and total chloride content near surface.

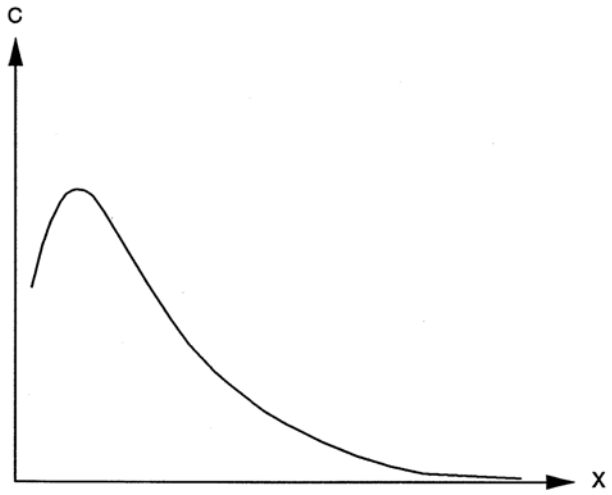

Figure 2.8 : Lower chloride content at the surface **(Nilsson et al., 1996)**.

The diffusion coefficient is affected by high aggregate content, which leads an increment by the tortuosity, at the same time increasing transition zone areas between paste and aggregate, which form the result that diffusion coefficients in concrete are higher than in the paste of the same composition. At the same time the physical properties of the capillary pore structure affects the diffusion rate significantly.

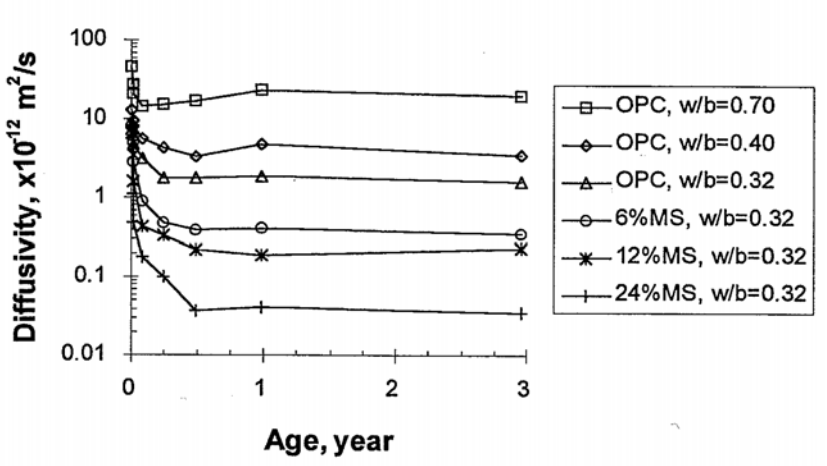

Figure 2.9 : The effect of degree of hydration on diffusivity **(Nilsson et al., 1996)**.

The age effect and maturity is also very important for diffusion. High degree of cement hydration cause a decrement of diffusion coefficient. Similarly, after the slow down of hydration, the diffusion coefficient remains constant. Other important factors are temperature and degree of saturation of concrete **(Nilsson et al., 1996)**.

The chloride diffusion is also a function of time and the change of chloride concentration with the time can be written with the help of the law of mass conservation;

$$\frac{\partial c}{\partial t} = -\frac{\partial F}{\partial x} \qquad \textbf{(2.19)}$$

where c is chloride concentration. When the first law of Fick (2.18) is substituted to (2.19), then the second law of Fick is formulated;

$$\frac{\partial c}{\partial t} = D\frac{\partial^2 c}{\partial x^2} \qquad \textbf{(2.20)}$$

The above differential equation can be solved for the boundary conditions of

$$\begin{aligned} c(x=0,t) &= c_s \\ c(x,t=0) &= 0 \end{aligned} \qquad \textbf{(2.21)}$$

where c_s is the surface chloride concentration and the solution becomes the common error function solution;

$$c(x,t) = c_s\left(1 - erf\left(\frac{x}{2\sqrt{D_a \cdot t}}\right)\right) \quad \textbf{(2.22)}$$

where the apparent diffusion coefficient D_a and surface chloride concentration c_s are found by curve fitting. The apparent diffusion coefficient is based on total species penetration and the effective diffusion coefficent is based on the penetration of the soluable component.

2.3.3 Chloride migration

An electrical field affects the movement of ions significantly, such that the movement is accelerated compared to pure diffusion, which means some ions move towards a concentration gradient. For large electrical potential gradients, the current produce a lot of heat, so the temperature of concrete raises. The total flow F of each ion was formulated by Nernst and Planck as

$$F_j = -D_j \frac{\partial c_j}{\partial x} + \frac{z_j F}{RT} D_j c_j \frac{\partial E}{\partial x} + c_j F_w \quad \textbf{(2.23)}$$

where E is the electrical potential, T is the absolute temperature, F is the Faraday number and R is the gas constant. The indices j and w stand for ion and water respectively. F_w is the flux of electrolyte, usually water. During the migration process the current carried by ions is converted into the current carried by electrons at the electrodes.

2.3.4 Combined chloride transport

2.3.4.1 Convection

A saturated water flow can move ions proportional to the flow and concentration of ions under pressure gradients. This transport is called convection.

$$F_{Cl} = \frac{c_f}{\rho_w} \cdot F_w \quad \textbf{(2.24)}$$

where c_f is free chloride concentration in pore water, ρ_w is the density of water and F_w is the flow of water.

2.3.4.2 Capillary suction

Capillary suction occurs when concrete has been dried to some level, water flows from a salt solution, which is in contact with concrete. It is denotable that capillary coefficient is dependent on the moisture distribution.

$$Q_{cl}(t) = \frac{c_f}{\rho_w} A\sqrt{t} \qquad \textbf{(2.25)}$$

In the above formula Q_{cl} represents the amount of chlorides sucked into the concrete in [kg/m^2], where c is the salt concentration in [kg/m^3], $t[s]$ is the duration of suction and A is the capillary coefficient in [kg/(m$^2\sqrt{}$s].

Chloride binding is a very important aspect during capillary suction, binding process filters the salt solution and the concentration of the penetrating salt solution drops with depth.

When suction ends, a further inwards moisture flow move chlorides deeper into the concrete. This movement stops below the critical moisture content, in fact the liquid paths become discontinuous and the evaporation at the surface cause a moisture flow to the surface.

2.3.4.3 Hydration suction

When the structure is exposed to salt solutions at the early-age, the salt may penetrate deep into the young concrete because of its high permeability. This process is called hydration suction.

2.3.4.4 Moisture flow and evaporation

A non-saturated water flow may cause internal evaporation. The migrating water evapourates and continues as water vapour flow. The chlorides will deposit at the site of that kind of evaporation causing the concentration of ions to increase. The increase in chloride content is proportional to the amount of evaporation but the distribution of chloride concentration is influenced by a certain counterdiffusion **(Nilsson et al., 1996)**.

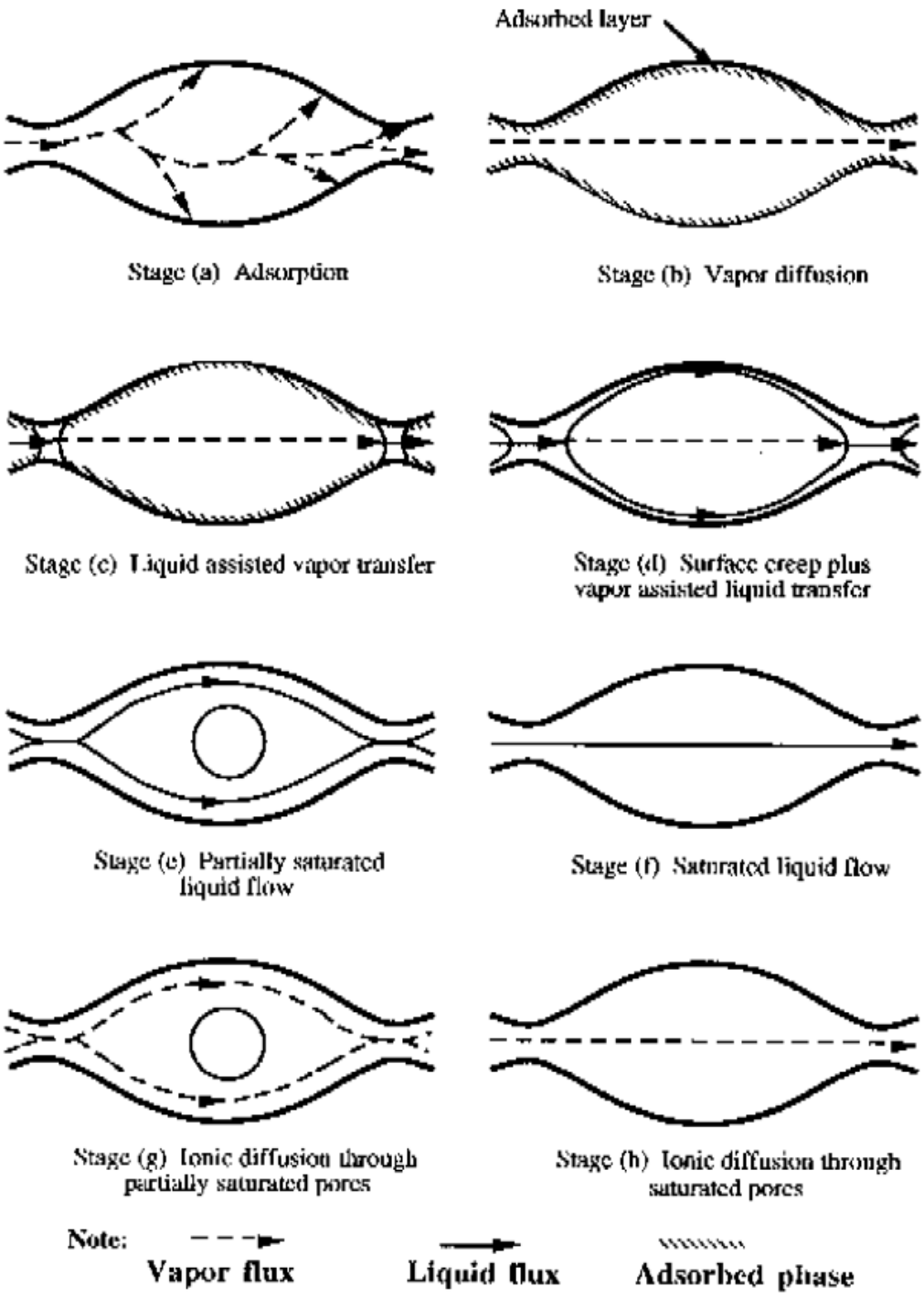

Figure 2.10 : Liquid and ionic transport processes **(Ramachandran et al., 2001)**.

3. METHODS FOR DETERMINATION OF PORE STRUCTURE

3.1 Mercury intrusion porosimetry (MIP)

Mercury intrusion porosimetry appears to be the most commonly used pore structure characterization technique. The method is straightforward and generally yields reproducible pore size distributions. Parameters such as the total porosity, the threshold diameter, the theoretical pore diameter, or the maximum continuous pore diameter and the mean pore diameter, can be deduced from these distributions **(Ramachandran et al., 2001)**.

MIP assume that the geometry of the pores is regular, that the pores are interconnected and that the size distribution is not affected by the loss of water in the pores upon drying.

The pore size distribution is determined from the volume intruded at each pressure increment. The continuous pore diameter, which is determined from the largest differential intruded volume with respect to diameter, identifies where percolation has occured. This diameter is called the threshold diameter **(Abell et al., 1999)**.

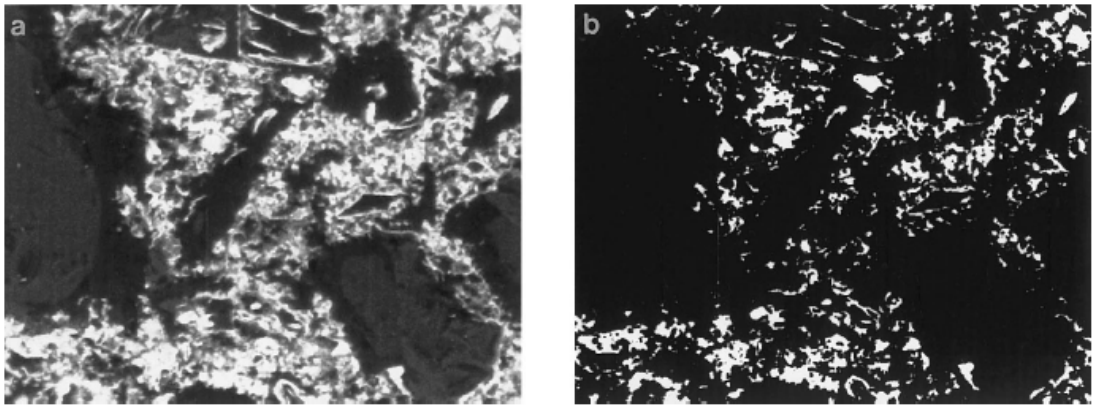

Figure 3.1 : Intruded mortar sample (a) Backscatter electron image (b) Binary image **(Abell et al., 1999)**.

However, despite its numerous advantages, the method is not believed to give the "true" pore size distribution of complex systems such as hydrated cement paste and concrete.

The threshold diameter is a valid parameter, related to permeability and ion diffusion in cement systems. On the other hand the intrudable porosity is not a measure of total porosity in the system, because the air voids, which are in sizes up to several

hundered micrometers are not filled with mercury until the threshold pressure is reached **(Diamond, 2000)**.

3.2 Air void analysis (AVA)

This test method determines the air content of hardened concrete and the air-void distribution of the air-void system in hardened concrete microscopically **(ASTM C 457, 1998)**. In an air void analysis, the entrapped and entrained air voids are investigated, because capillary pores are submicroscopic and cannot be measured via microscopic methods.

Entrapped voids are unintentionally included, or entrapped, within the concrete during the mixing and placement process. They are relatively large to all other air voids and are distinguished easily from other voids by size and shape. Entrained air voids are added intentionally into the concrete with the help of air entraining admixtures and they are formed spherical.

A reliable analysis is realized if and only if the sample is well prepared. The best result is obtained if there is a maxiumum contrast between the air voids and the rest of the sample.

The air void content determined in accordance with the test method **ASTM C 457 (1998)** usually agrees closely with the value determined on the fresh concrete. However, some differences may be obtained if the fresh concrete sample is consolidated to a different degree.

3.2.1 Air content

The proportion of the total volume of the concrete that is air voids; expressed as percentage by volume.

4. METHODS FOR DETERMINATION OF CONCRETE PERMEABILITY

4.1 Diffusion tests

The transport of either gas, water vapour, or ion, due to a concentration gradient across concrete can be used to determine its diffusion characteristic. Diffusion tests can be classified as:

1. Gas diffusion

2. Water vapour diffusion

3. Ionic diffusion

4.1.1 Gas diffusion tests

In this method, two streams of gas of equal pressure and temperature are passed through either side of the specimen, therefore, the transfer of gases by diffusion is stimulated by a difference in concentration. Traces of one gas are detected in the stream of the second gas (which is normally an inert gas) to measure the rate of gas diffusion through the specimen.

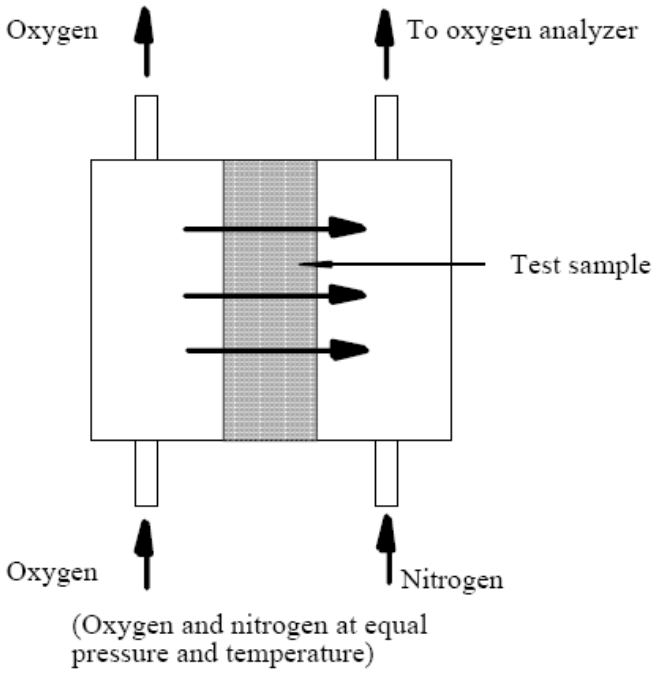

Figure 4.1 : Gas diffusion test setup **(Ramachandran et al., 2001)**.

4.1.2 Water vapour diffusion tests

The water vapour diffusion tests can be considered under water vapour transmission tests and water vapour transpiration tests. In water vapour transmission tests, the water vapour passing through the specimen is collected, either by condensing it or by absorbing with a desiccant. In water vapour transpiration tests, the loss of weight of a saturated specimen due to the breathing (evaporation of water from concrete) is measured.

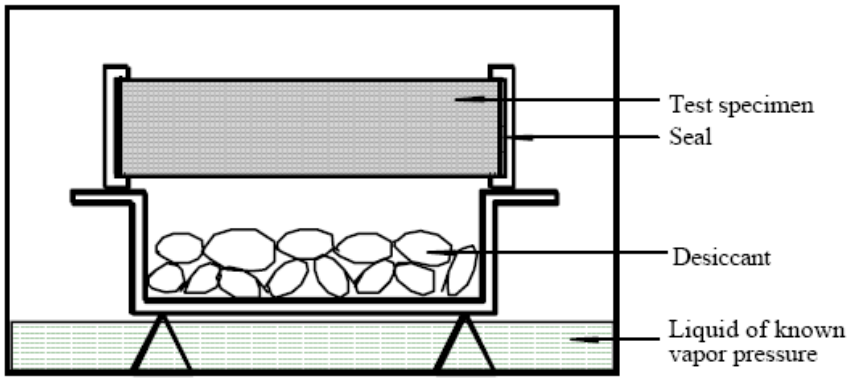

Figure 4.2 : The dry cup method for water vapour transmission test **(Ramachandran et al., 2001)**.

4.1.3 Ionic diffusion tests

The transport of ions in concrete involves diffusion, capillary suction, and convective flow, with flowing water, accompanied by physical and chemical binding, depending on the physical environmental conditions. In order to determine the ionic transport, these complications are usually neglected, and pure diffusion, sometimes with binding capacity, is adopted. Pure diffusion of ions in the pore solution of a concrete occurs due to differences in the concentration of the ions. Therefore, concrete should be matured and saturated and there should be no movement of water or carbonation of concrete during the test.

The chloride diffusion coefficient can be determined from several types of tests and, on the basis of the methodology used, these tests can be classified as:

1. Steady state diffusion tests

2. Non-steady state diffusion tests

3. Electric field migration tests

Another type which can be included under ionic diffusion test is the use of resistivity methods; however, these do not measure ionic transport directly.

4.1.3.1 Steady state diffusion tests

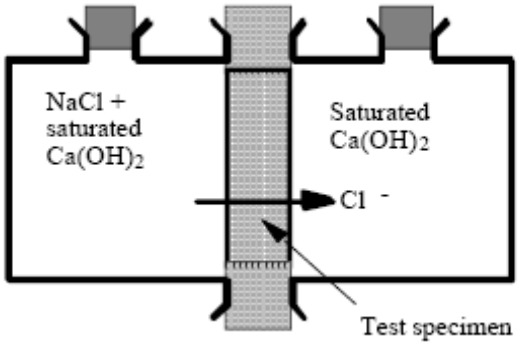

Figure 4.3 : Ion diffusion cell **(Ramachandran et al., 2001)**.

In steady state diffusion tests, a thin slice of the test specimen forms a barrier between an ion rich solution and another suitable solution free of ions. This allows ions to diffuse in a concentration gradient. The rate of diffusion is obtained by periodically determining the ion content in the ion-free solution. When steady state conditions are achieved, the diffusion coefficient is calculated by using Fick's first law of diffusion **(Eq.2.18)**.

4.1.3.2 Non-steady state diffusion tests

In non-steady state diffusion tests the penetration of ions is achieved either by immersing the specimen in a solution containing specific ions for a certain time or by ponding the solution containing specific ions on the test specimen for a certain time. The penetration is maintained unidirectional by sealing all except one surface of the specimen. Either the penetration depth or the penetration profile of the specific ions in the specimen is determined and Fick's second law of diffusion is applied to determine the diffusion coefficient **(Eq.2.20)**.

The diffusion coefficient varies with the concentration of solution on the exposed surface and the duration of exposure due to the variation in binding capacity of concrete at different environmental conditions. Therefore, the diffusion coefficient, by assuming that it remains constant for the material, has to be treated as an apparent diffusion coefficient **(Ramachandran et al., 2001)**.

4.1.3.2.1 Immersion test

This is a longterm test, which is standardized as NT BUILD 443 test. The test specimen is first immersed in saturated calcium hydroxide solution until constant mass is achieved, in order to prevent capillary suction of exposure liquid during the test. The specimen is then immersed in the exposure liquid for a period of at least 35 days at a constant temperature. At the end of the exposure period the penetration profile is determined and the diffusion coefficient is calculated **(Ramachandran et al., 2001)**.

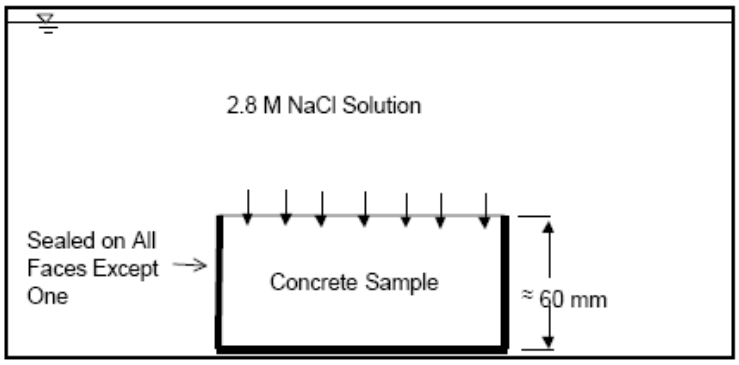

Figure 4.4 : A typical immersion test setup **(Stanish et al., 1997)**.

4.1.3.2.2 Salt ponding test

This is a longterm test, which is standardized as AASHTO T259 test. Test specimens with a dyke at the top to pond a 3% (0.5 M) sodium chloride solution continuously for a period of 90 days. At the end of this exposure period, the solution is removed and the concrete is sampled at various depths by using a 25 mm diameter rotary hammer drill. The total chloride ion content of each sample is analyzed and plotted against the depth of sampling. The area under the chloride profile is calculated and reported as the total chloride content **(Ramachandran et al., 2001)**.

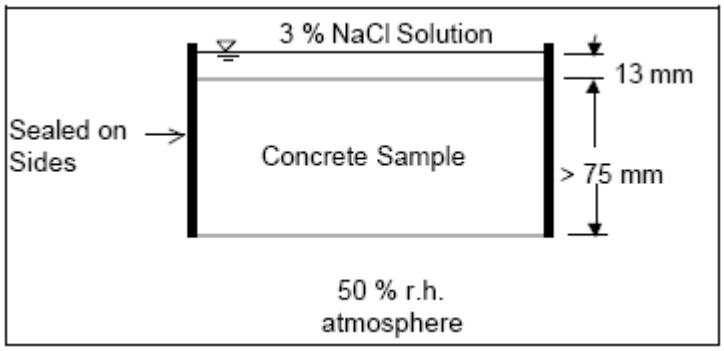

Figure 4.5 : A typical salt ponding test setup **(Stanish et al., 1997)**.

4.1.3.3 Electric field migration tests

Steady state and non-steady state diffusion tests are very time-consuming methods. In order to get results quickly, methods where the transport of ions can be accelerated by the application of electrical potential gradients have become very popular recently. These tests are called electrical migration tests **(Ramachandran et al., 2001)**.

4.1.3.3.1 Rapid chloride permeability test

This test method covers the determination of the electrical conductance of concrete to provide a rapid indication of its resistance to the penetration of chloride ions. This test method is applicable to types of concrete where correlations have been established between this test procedure and longterm chloride ponding procedures such as those described in AASHTO T 259 **(ASTM C 1202, 2005).**

The test uses a 50 mm thick and 95 mm diameter specimen. The specimen is vacuum saturated for 18 hours and enclosed between two chambers, one containing a solution of 3% by weight sodium chloride and the other with 0.3 M NaOH solution. An electric field of 60V direct current is applied between the electrodes in each chamber. The test is run for 6 hours and during that time the amount of charge passing the specimen is measured by recording the current as a function of time. The total charge passed through the specimen, in coulombs, is determined by calculating the area under the current-time plot during the 6 hour test period.

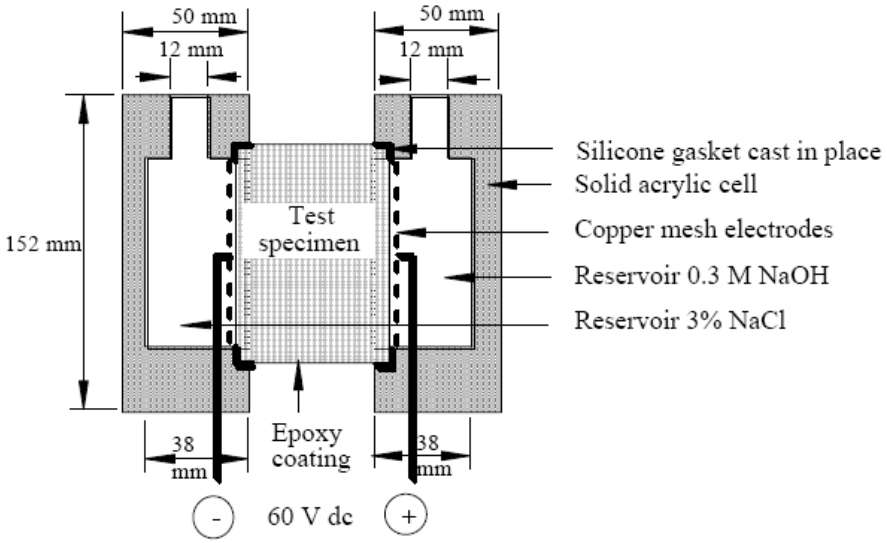

Figure 4.6 : ASTM C1202 test setup **(Ramachandran et al., 2001)**.

Some criticism has been directed towards this test method, since the total charge refers to the movement of all ions present in the pore solution rather than the flux of chlorides, different binders may not provide the same classification criteria. Another objection has been that when integrating the total current from the beginning of the experiment it does not distinguish between chloride flow plus reaction or simple flow. The information from this test could be obtained by measuring the initial resistivity within a test period of a few seconds **(Ramachandran et al., 2001)**.

4.1.3.3.2 Rapid migration test (CTH test)

Tang and Nilsson proposed a variation on the conventional migration cell unique enough to be mentioned separately. A migration cell is set up with a specimen 50 mm thick and 100 mm in diameter, and an applied voltage of 30 V, as shown in **Figure 4.7**.

The experiment proceeds as usual for an electrical migration test, except that the chloride concentration of the downstream solution is not monitored. Instead, after a specified duration (Tang and Nilsson used 8 hours) the samples are removed and split, and the depth of chloride penetration is determined in one half of the specimen using a colorimetric technique in which a silver nitrate solution is used as a colorimetric indicator. When a silver nitrate solution is sprayed on a concrete the chlorides bind with the silver to produce silver chloride, a whitish substance. In the absence of chlorides, the silver instead bonds with the hydroxides present in the concrete, creating a brownish color. The penetration depth is used to determine a chloride ion diffusion coefficient using the Nernst-Einstein equation **(Eq.2.23) (Ramachandran et al., 2001)**.

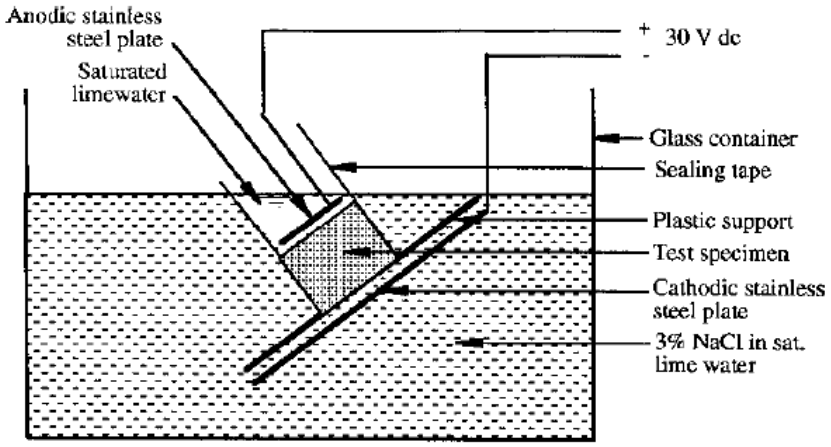

Figure 4.7 : Rapid migration test setup **(Ramachandran et al., 2001)**.

4.2 Absorption tests

The penetration of liquids in concrete as a result of capillary forces which allow a wetting fluid to be drawn along the solid-pore surface is absorption. The measurement of absorption characteristics of concrete can be classified into three categories:

1. Tests for water absorption capacity

2. Sorptivity tests

3. Absorptivity tests

In the absence of any external force the basic mechanism that drives water in capillary pores in concrete is capillary suction (capillarity). Surface tensional forces acting at a solid-liquid-gas interface cause a wetting liquid, such as water, to spread along the solid surface and results in capillary rise of the liquid in the capillary pore. Therefore, the capillary transport is theoretically dependent on the viscosity, density, and surface tension, of the liquid, the angle of contact between the solid and the liquid, the length of the pore already filled with the liquid, and the radius of the capillary pore.

4.2.1 Capillary water absorption test

The test specimen of uniform cross section is placed with one surface just in contact with water and the weight of water absorbed by capillary rise is measured at fixed intervals. After obtaining at least five data points, a graph is plotted between the volume of water absorbed per unit area of inflow surface and square root of time. The slope of this plot is reported to be the sorptivity of the material.

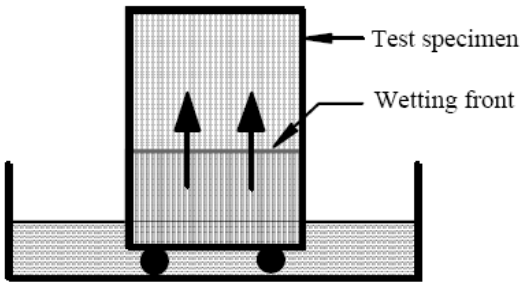

Figure 4.8 : Capillary water absorption test setup **(Ramachandran et al., 2001)**.

4.2.2 Initial surface absorption test

The rate of flow of water into concrete per unit area after a stated interval from the start of the test and at a constant applied head and temperature is defined as initial surface absorption.

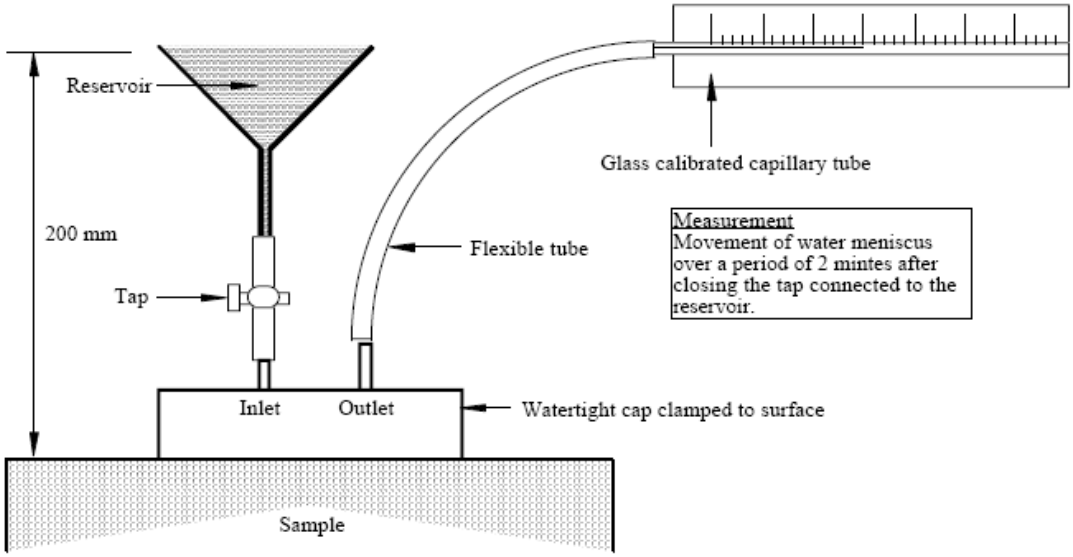

Figure 4.9 : Initial surface absorption test setup **(Ramachandran et al., 2001)**.

4.3 Permeability tests

These tests provide a means for measuring the true permeability. The basic requirement is that a specimen, usually a core, should be sealed on its curved face so that between its two opposite paralel faces the flow of a liquid or a gas can be promoted by an applied pressure. Under steady state conditions the coefficient of permeability is calculated from a knowledge of sample geometry and fluid characteristics, and the measurement of flow rate and applied pressure. The permeability tests are broadly classified as liquid permeability tests and gas permeability tests.

4.3.1 Steady state water flow test

The test determines the rate of flow of water at the steady state condition for a given test pressure and sample geometry. Using this data, the coefficient of water permeability or the intrinsic permeability can be determined. If the test specimen is

fully saturated with water and there are no chemical or physical interactions between concrete and water during the test, then the permeability is obtained as the intrinsic permeability of the concrete.

Permeability cells of various specifications and dimensions exist in order to apply water under pressure to one side of the specimen and measure the rate of flow either at the inlet or at the outlet or sometimes at both ends. The type of test specimen, test pressure, duration of the test, and the method used to seal the specimen in the cell, are the effective factors influencing the results **(Ramachandran et al., 2001)**.

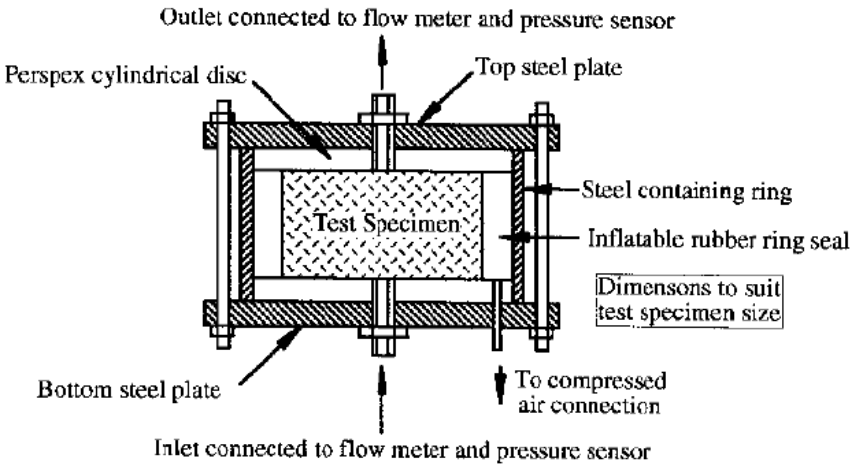

Figure 4.10 : Permeability cell **(Ramachandran et al., 2001)**.

4.4 Light intensity test

In recent years, optical fluorescence microscopy of concrete has been used as a tool to investigate the internal structure of hardened concrete. The method used in concrete petrography has been borrowed from geology and it is based on vacuum impregnation of concrete using a yellow fluorescent epoxy **(Akyüz et al., in press)**. During impregnation the capillary porosity, cracks, voids, and defects in the concrete are filled with epoxy. After impregnation, thin sections are prepared from slices of concrete that are attached to a glass slide, and then ground to a thickness of about 20μm to 30μm **(DS 423.40, 2002)**.

Thin sections allow the concrete petrographer to identify the material constituents and predict their proportions, air content, water-cement ratio, paste homogeneity, paste volume, aggregate volume, effectiveness of curing, and examine the relationships between the various constituents. The impregnation depth of the fluorescent epoxy into the sample is dependent on the capillary porosity of the

cement paste **(Laugesen, 1993)**. Large cracks, cement paste-aggregate debonding, interconnected porosity, and air voids can be easily impregnated.

5. EXPERIMENTAL WORK

The experimental phase is divided in two parts. Firstly, the early-age hydration properties of cement paste and mechanical properties of concrete were investigated. Secondly several methods were performed for the determination of the permeability of hardened concrete.

5.1 Hardening concrete

In the early age investigation, two types of binder paste with differing water to cement ratios were cast and the relative degree of hydration of 1 day, 3 and 7 days to the 28 days degree of hydration were determined. Additionally, gel to space ratios of all paste samples are computed. Concrete specimens were cast for compressive strength, rapid chloride permeability and chloride diffusion tests, adiabatic heat development test and petrographic examination with the same water to cement ratio and binder properties. The petrographic examination was performed on thin sections.

5.1.1 Materials

Oyak Cement CEM I 42.5, Tuncbilek fly ash and Elkem microsilica were used as binders to cast paste and concrete samples. The properties of these binders are listed on **Table 5.1**. and the binder paste mixture proportions are shown on **Table 5.2**.

For concrete samples Ergören natural sand, Koç crushed sand and Koç coarse aggregates were used in all mixtures. The aggregate mixture proportions and grading results are shown on **Table 5.3**. Additionally, Glenium Sky 506M and MicroAir 200B were used as superplasticizer and air-entraining admixtures in concrete.

The cement content was specified as 320 kg/m^3. The solid content of the microsilica slurry is 51%, which indicates that 15 kg is solid microsilica of 29.4 kg microsilica slurry. The concrete mixture proportions are shown on **Table 5.4**.

Table 5.1: Chemical and physical properties of binders

Components	**Cement**	**Fly ash**	**Microsilica**	**[unit]**
Water content	-	-	0.53	%
Dry matter	-	-	99.47	%
Loss on ignition	1.20	1.16	2.21	%
SiO_2	21.21	56.04	-	%
Al_2O_3	4.30	19.09	-	%
Fe_2O_3	5.70	9.57	-	%
CaO	62.37	3.81	-	%
MgO	1.20	5.97	0.42	%
C_3A	1.75	-	-	%
SO_3	2.83	0.79	0.13	%
TiO_2	-	0.79	-	%
Free CaO	0.65	0.03	0.01	%
Reactive SiO_2	-	43.28	91.00	%
Na_2O	0.11	0.48	0.10	%
K_2O	0.43	1.75	0.54	%
Na_2O equivalent total alkali	0.39	1.68	0.46	%
Cl^-	0.0055	0.0011	0.0470	%
Density	3.24	2.21	2.21	g/cm^3
Specific surface	3880	-	-	cm^2/g
Initial setting time	180	-	-	min
Final setting time	240	-	-	min
28-day activity index	-	77.0	-	%

Table 5.2: Binder paste mixture proportions by weight percentage of cement

CODE	w/c	0.35	0.40	0.45	0.50	0.55
C	Water	0.35	0.40	0.45	0.50	0.55
SF	Fly ash	0.18	0.18	0.18	0.18	0.18
	Microsilica	0.05	0.05	0.05	0.05	0.05
	Water	0.41	0.46	0.52	0.58	0.64

Table 5.3: Aggregate mixture proportions and grading results

Aggregates	Mix	Grading [mm]									
	%	31,5	16	8	4	2	1	0,5	0,25	0,125	0,063
Coarse agg. 2	25	100	55	1	0	0	0	0	0	0	0
Coarse agg. 1	25	100	100	54	2	1	1	1	1	1	1
Crushed sand	15	100	100	100	88	53	29	15	7	3	2
Natural sand	35	100	100	100	100	97	85	59	25	4	1
TOTAL	100	100	89	64	49	42	35	23	10	2	1

Table 5.4: Concrete mixture proportions in kg/m^3

CODE	C1	C2	C3	C4	C5	SF1	SF2	SF3	SF4	SF5
w/c	0.35	0.40	0.45	0.50	0.55	0.35	0.40	0.45	0.50	0.55
Cement	320	320	320	320	320	275	275	275	275	275
Fly ash	0	0	0	0	0	50	50	50	50	50
Microsilica slurry	0	0	0	0	0	29.4	29.4	29.4	29.4	29.4
Water	108.6	124.6	140.6	156.6	172.6	94.2	110.2	126.2	142.2	158.2
Natural sand	660.8	646.2	631.7	617.1	602.6	646.2	631.6	617.0	602.5	587.9
Crushed sand	295.2	288.7	282.2	275.7	269.2	288.6	282.1	275.6	269.1	262.6
Coarse agg. 1	490.1	479.3	468.5	457.7	446.9	479.3	468.5	457.7	446.9	436.1
Coarse agg. 2	495.6	484.7	473.8	462.8	451.9	484.6	473.7	462.8	451.9	440.9
Super plasticizer	12.12	5.82	3.44	1.59	0.74	10.88	5.47	2.82	0.97	0.56

5.1.2 Degree of hydration

One set was cast only with cement and water, and the other set was cast with cement, fly ash, microsilica slurry and water. Both sets have the same equivalent cement content according to the formula

$$C_{equivalent\ cement} = C_{cement} + 0.3C_{fly\ ash} + 2C_{microsilica\ (solid)} \ . \qquad \textbf{(5.1)}$$

After achieving the required age, samples for the non-evapourable water content determination were ground to powder and washed with acetone in order to stop the hydration. They were placed in crucibles of known mass and left for 20 hours in an oven at 105°C. When they were removed from the oven, the masses of the samples were redetermined and then placed in a furnace at 1000°C for a minimum of 4 hours, after which their masses were determined once again. The non-evapourable water content was calculated as the difference between the 1000°C and 105°C mass measurements divided by the mass of cement remaining at 1000°C and corrected for the losses on igniton of cement, fly ash and slurry samples as **Bentz (1997)** stated before.

5.1.3 Compressive strength

Concrete samples were cast with the same binder proportions and water to cement ratios as mentioned in the paragraph **5.1.1** above and shown on **Table 5.4**, which were loaded under compression according to the **TS EN 12390-3 (2003)**. The tests were performed on the 1st, 3rd and 7th days after casting.

5.1.4 Adiabatic heat development test

Concrete samples were kept in an insulated container. The generated heat is partly used to raise the temperature in the concrete and partly lost by convective heat transfer from the concrete to the surroundings (into and through the insulation). The amount of heat generated is determined as the sum of the heat accumulated in the concrete and the heat lost to the surroundings. The temperature rise in the concrete is used as a measure of the accumulated heat, and a temperature transducer built into the insulation wall of the container is used to yield a measure of the heat loss **(NT BUILD 388, 1992)**.

A haybox calorimeter is a suitable insulated box equipped with devices to measure the temperature in the concrete as shown in **Figure 5.1** and a property that can be correlated to the heat loss from the concrete through a calibration factor.

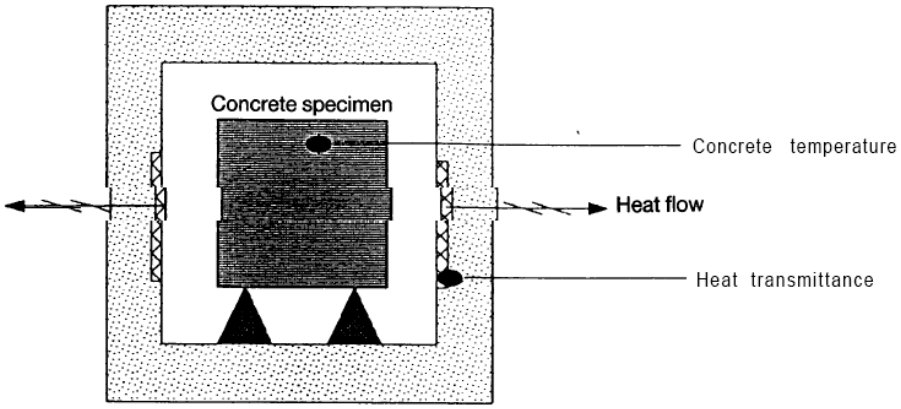

Figure 5.1 : Haybox calorimeter **(NT BUILD 388, 1992)**.

The data provided from the datalogger was put into a calculation sheet in order to compute the accumulated heat and the rate of that heat versus maturity of the concrete **(DTI, 2003a)**. The obtained results were put into the 4C Temp&Stress software **(DTI, 2003b)** to make linear and exponential regressions in order to estimate the accumulated heat at infinity.

5.1.5 Chloride permeability test

The rapid chloride permeability tests were performed according to **ASTM C 1202 (2005)** again for early-age samples on the 1st, 3rd and 7th days after casting. But it must be denoted, that some tests were not completed, because the datalogger turned off automatically for safety reasons due to high temperature and/or high current rates, which were appeared during testing.

5.1.6 Thin section analysis

Thin sections were prepared for each mix design when the required age is achieved, namely on the 1st, 3rd and 7th days after casting. The method to stop the hydration is the same method, which is mentioned in the degree of hydration paragraph. Concrete samples were immersed to acetone bath and kept for 24 hours. It must be also denoted, that some thin sections were badly damaged during sawing. Pull-outs and scratches appeared on the samples due to very low strength at the first day after casting.

The analysis was performed under the 50x magnification of a polarized microscope according to the Danish standards, **DS 423.41~DS 423.45 (2002)**.

5.1.7 Chloride diffusion

A water-saturated concrete specimen is, on one plane surface, exposed to water containing sodium chloride. After 35 days of exposure time, thin layers are ground off parallel to the exposed face of the specimen and the chloride content of the layers, C_x, is measured by potentimetric titration. The original (initial) chloride content of the concrete, C_i, is measured at a suitable depth below the exposed surface. The effective chloride transport coefficient, De, and the boundary condition of the chloride profile at the exposed surface, Cs, are calculated by non-linear regression at MATLAB. The penetration parameter, K_{Cr} , is calculated for a selected chloride concentration, Cr **(NT BUILD 443, 1995)**.

5.2 Hardened concrete

In this part of the experimental work, compressive strength, rapid chloride permeability, capillary water absorption and air void analysis were performed. Air void analysis and capillary water absorption tests will be explained in detail in further paragraphs.

Table 5.5: Chemical and physical properties of Nuh Cement

Components	Cement	[unit]
Loss on ignition	1.88	%
SiO_2	20.66	%
Al_2O_3	4.17	%
Fe_2O_3	3.67	%
CaO	64.08	%
MgO	1.05	%
C_3A	4.84	%
SO_3	3.14	%
Na_2O	0.16	%
K_2O	0.58	%
Na_2O equivalent total alkali	0.54	%
Cl^-	0.0064	%
Density	3.17	g/cm^3
Specific surface	3170	cm^2/g
Initial setting time	155	min
Final setting time	210	min

Table 5.6: Concrete mixture proportions of CON1 in kg/m^3

CODE	CON1-C					CON1-SF				
w/c	0.35	0.40	0.45	0.50	0.55	0.35	0.40	0.45	0.50	0.55
Cement	320	320	320	320	320	275	275	275	275	275
Fly Ash	0	0	0	0	0	50	50	50	50	50
Microsilica slurry	0	0	0	0	0	29.4	29.4	29.4	29.4	29.4
Water	108.6	124.6	140.6	156.6	172.6	93.7	109.7	125.7	141.7	157.7
Natural sand	658.3	643.7	629.2	614.7	600.2	637.2	622.8	608.5	594.1	579.8
Crushed sand	295.2	288.7	282.2	275.7	269.2	286.9	280.5	274.0	267.5	261.1
Coarse agg.1	495.6	484.7	473.8	462.8	451.9	486.2	475.2	464.3	453.3	442.4
Coarse agg.2	492.0	481.1	470.3	459.4	448.6	488.2	477.2	466.2	455.2	444.2
Super plasticizer	4.78	4.78	2.02	0.93	0.83	4.78	2.41	2.00	1.53	0.78

5.2.1 Materials

For this section 4 sets of concrete were cast. CON1 sets include binders, aggregates and admixtures, which were mentioned in **5.1.1**. The CON1 mixture proportions are shown on **Table 5.6**.

CON2 sets include only Nuh Cement CEM I 42.5 as binder, which has the following properties shown in **Table 5.5** above. Ergören natural sand, Kancataş crushed sand and Kancataş coarse aggregates were used in CON2 mixtures. The aggregate mixture proportions and grading results of CON2 concretes are shown on **Table 5.7**. Additionally, Glenium ACE30 was used as superplasticizer in concrete.

Table 5.7: Grading results

Aggregates	Mix	Grading [mm]									
	%	31,5	16	8	4	2	1	0,5	0,25	0,125	0,063
Coarse agg. 2	20	100	62	1	1	1	1	1	1	1	1
Coarse agg. 1	25	100	100	54	2	1	1	1	1	1	1
Crushed sand	25	100	100	100	92	49	30	14	7	3	2
Natural sand	30	100	100	100	100	93	79	53	22	6	3
TOTAL	100	100	92	69	54	41	32	20	9	3	2

The cement content of CON2 concrete was specified as 450 kg/m^3 and the concrete mixture proportions are shown on **Table 5.8**.

Table 5.8: Concrete mixture proportions of CON2 in kg/m^3

CODE	CON2-C1					CON2-C2				
w/c	0.30	0.35	0.40	0.45	0.50	0.30	0.35	0.40	0.45	0.50
Cement	450	450	450	450	450	450	450	450	450	450
Fly Ash	0	0	0	0	0	0	0	0	0	0
Microsilica slurry	0	0	0	0	0	0	0	0	0	0
Water	132.7	155.2	177.7	200.2	222.7	132.7	155.2	177.7	200.2	222.7
Natural sand	544.8	527.6	510.4	493.2	476.0	544.8	535.9	518.4	500.9	483.4
Crushed sand	478.9	463.8	448.7	433.6	418.4	478.9	464.2	449.0	433.9	418.7
Coarse agg.1	478.9	463.8	448.7	433.6	418.4	478.9	469.7	454.4	439.0	423.7
Coarse agg.2	384.6	372.4	360.3	348.1	336.0	384.6	376.0	363.8	351.5	339.2
Super plasticizer	4.04	2.68	1.275	0.31	0	3.38	2.22	2.22	2.20	0.52

5.2.2 Capillary water absorption

This test method was used to determine the rate of sorptivity of water by hydraulic cement concrete by measuring the increase in the mass of a specimen resulting from absorption of water as a function of time when only one surface of the specimen is exposed to water. The exposed surface of the specimen is immersed in water and water ingress of unsaturated concrete dominated by capillary suction during initial contact with water **(ASTM C 1585, 2004)**. At this work, specimens were tested at 126 days.

5.2.3 Air void analysis

The specimen is polished according to the ASTM C 457 and the surface become plane and smooth without saw marks. Then the surface is coloured with black or any other dark marker. When the specimen totally absorps the colour, a white zinc paste (a mixture of zincoxide powder and vaseline) is applied to the surface to fill the air voids **(Figure 5.2)**. Excess zinc paste is removed and the surface is rubbed with

mineral oil. In the final step voids in aggregates and cracks are also coloured under the stereomicroscope.

At this work, specimens were tested at 134 days. Prepared specimens are analyzed automatically with CXI Air Void Analyzer 457. The analysis was applied with the linear traverse method for a 2413 mm long distance. The analysis was performed four times on each specimen, by rotating samples 90° degree after each analysis.

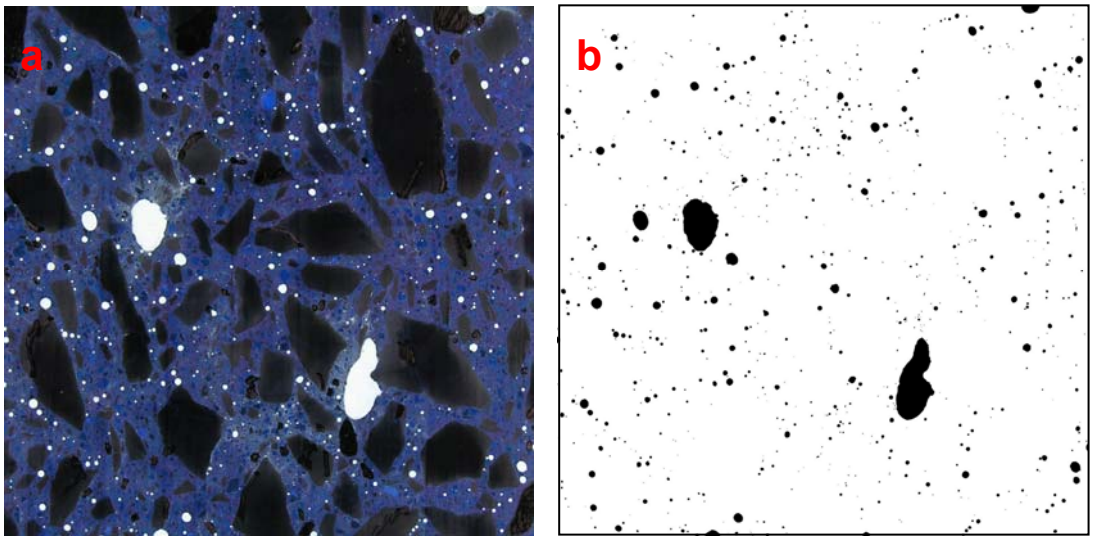

Figure 5.2 : Appeareance of AVA sample (a) after being coloured and filled with white zincpaste (b) inversely scanned image, air voids appear black

6. RESULTS AND DISCUSSION

Hydration degree results are shown in graphics relative to the 28 days of hydration results. In **Figure 6.1** and **Figure 6.2**, hydration degree values are close to each other, both in only cement paste samples and cement-flyash-microsilica samples.

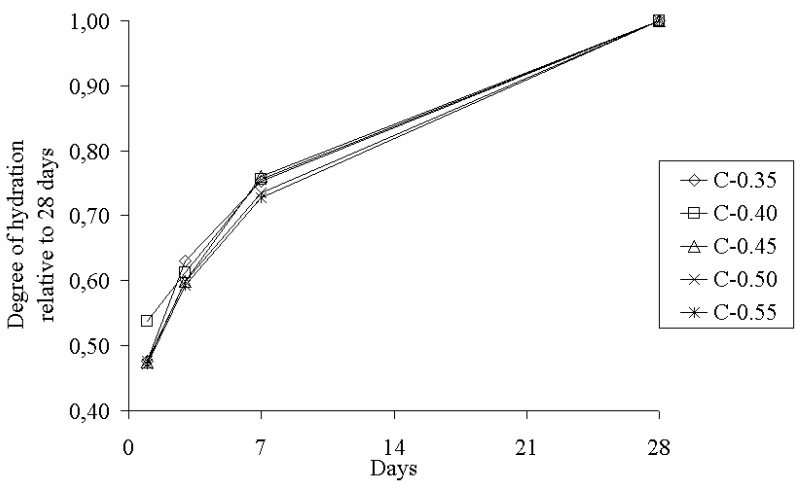

Figure 6.1 : Time vs. degree of hydration for cement paste (C) samples

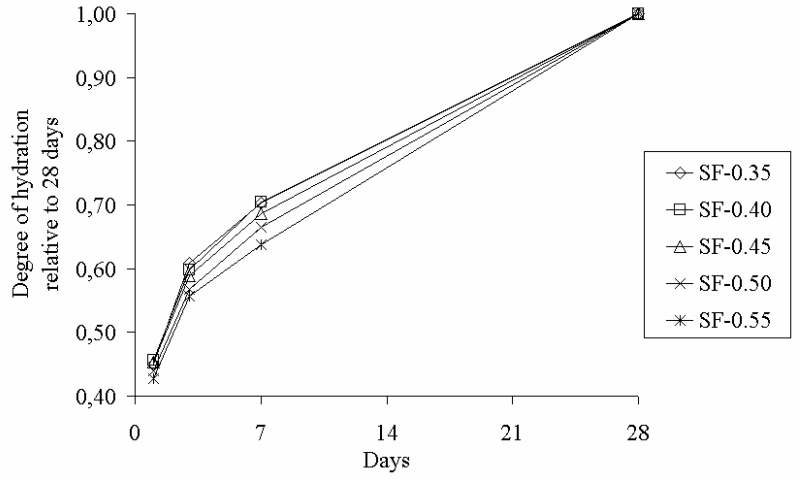

Figure 6.2 : Time vs. degree of hydration for cement-flyash-microsilica (SF) paste samples

It is obtained from **Figures 6.1** and **6.2** that, the degree of hydration decreases, when w/c ratio increases. **Figure 6.3** relates w/c ratio to the degree of hydration, where the hydration degree of cement paste samples are higher than to cement-flyash-microsilica samples. This figure shows dramatically, how mineral additives can affect the hydration process.

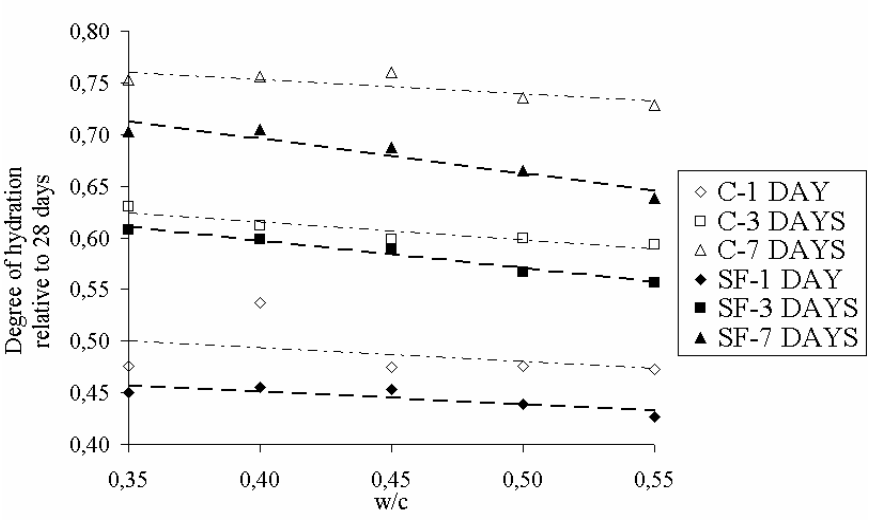

Figure 6.3 : w/c vs. degree of hydration

From the hydration degree test results of C and SF pastes, gel to space ratio values are calculated by using the **Eq.2.15** and **Eq.6.1** and are shown on **Table 6.1**.

$$X_{SF} = \frac{2.06\nu_C\alpha_C c + 2.52\nu_F\alpha_F f + 2.52\nu_M\alpha_M m}{\nu_C\alpha_C c + \nu_F\alpha_F f + \nu_M\alpha_M m + w} \qquad \textbf{(6.1)}$$

where X_{SF} is the gel/space ratio of SF pastes; ν_C, ν_F and ν_M are the specific volumes, and α_C, α_F and α_M are the degrees of reaction of cement, fly ash and microsilica respectively; c, f and m are the original fractions of cement, fly ash and microsilica in the SF blend on an ignited basis; and w is the weigth of water mixed with per gram of ignited SF blend.

Table 6.1: Gel to space ratio values of C and SF pastes

	Days	0,35	0,40	0,45	0,50	0,55
C	1	0,474	0,485	0,400	0,376	0,347
	3	0,585	0,536	0,481	0,454	0,419
	7	0,663	0,625	0,576	0,531	0,492
	28	0,799	0,754	0,697	0,662	0,622
SF	1	0,489	0,492	0,425	0,401	0,373
	3	0,606	0,560	0,514	0,485	0,453
	7	0,682	0,646	0,602	0,561	0,522
	28	0,832	0,791	0,744	0,713	0,677

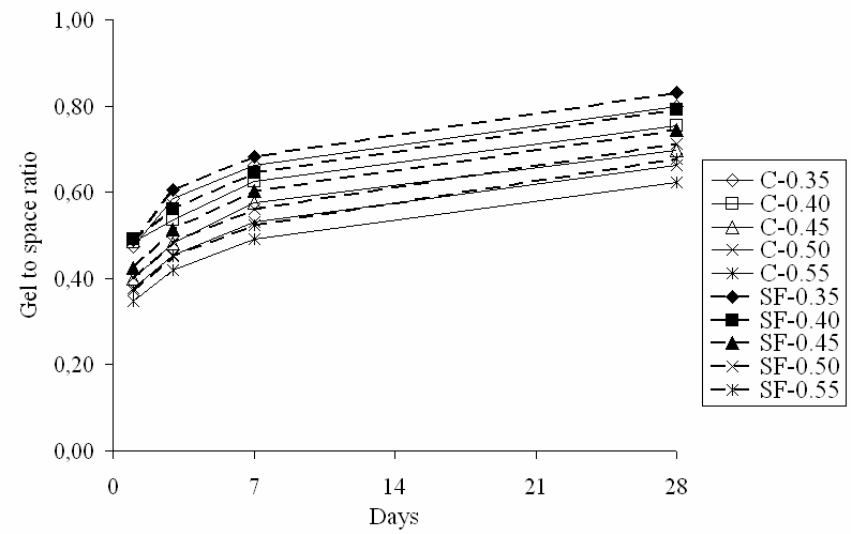

Figure 6.4 : Time vs. gel to space ratio for paste samples

Figure 6.4 visualizes the values on **Table 6.1.** It is obtained that gel/space ratio increases with time. An increase in the water to cement ratio causes a decrement in the gel to space ratio. Another result is that SF pastes have higher gel/space ratio values than C pastes at the same water to cement ratios. This can be explained with the output substances after hydration. 1 ml of hydrated cement occupies 2.06 ml, while 1 ml of reacted fly ash occupies 2.52 ml of space. Therefore SF pastes fill in the space denser than C pastes, because of filling effect and pozzolanic reactions of mineral admixtures **(Lam et al., 2000)**.

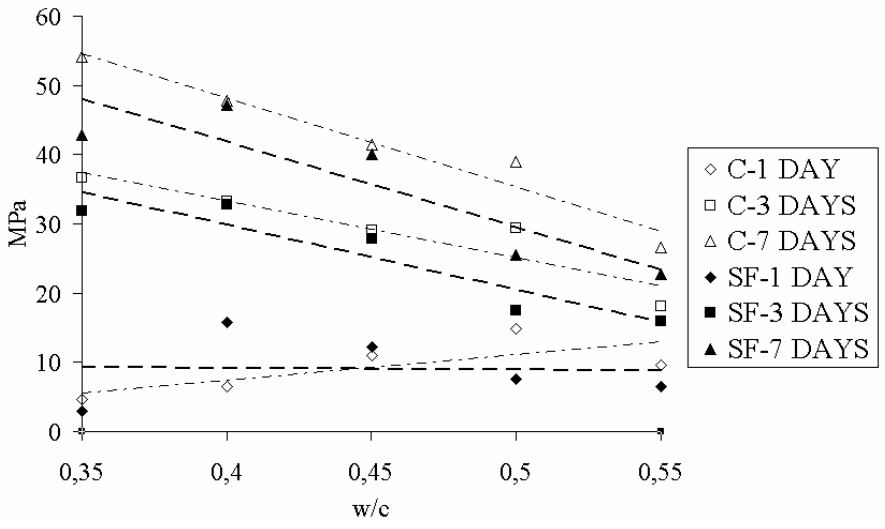

Figure 6.5 : w/c vs. compressive strength in hardening concrete

Figure 6.5 shows the well-known relationship of w/c vs. compressive strength. When w/c ratio increases, the compressive strength decreases. If it is compared with the previous figure, that the strength developments are parallel to hydration degree developments. It is derivable that strength is a result of hydration.

As mentioned in paragraph **5.1.5**, that some tests were not completed for the rapid chloride permeability test according to ASTM C 1260, because the datalogger turned off automatically for safety reasons due to high temperature and/or high current rates, which were appeared during testing. This problem affected the results very much, and it can not be obtained any permeability trend for the samples with varying w/c ratio and time as shown in **Figure 6.6**.

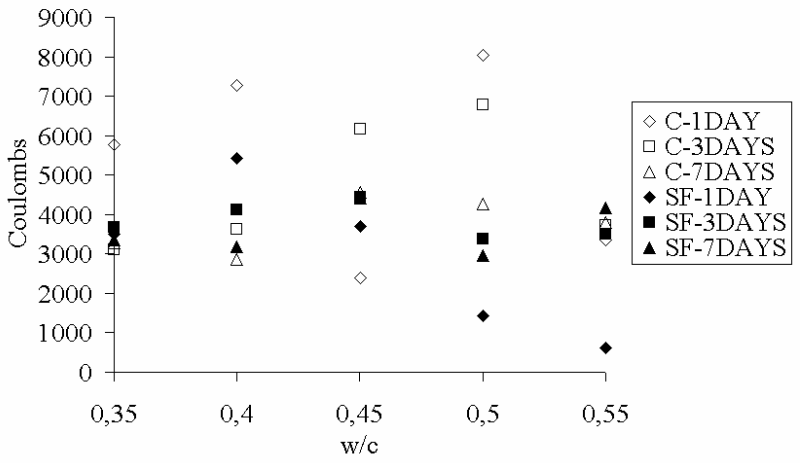

Figure 6.6 : w/c vs. charge passed in hardening concrete

As stated in paragraph **4.4** petrographic techniques also help researchers by determining the microstructural properties of concrete. At this work, thin sections, which were prepared from concrete samples shown in **Table 5.4**, are analyzed according to Danish standards **DS 423.41~DS 423.45 (2002)**. Photos were captured from each sample and put into the W-C Check software to measure the luminosity of them. Captured photos are shown in **Figures 6.7** and **6.8** and the measurements are shown in graphics in **Figure 6.9**.

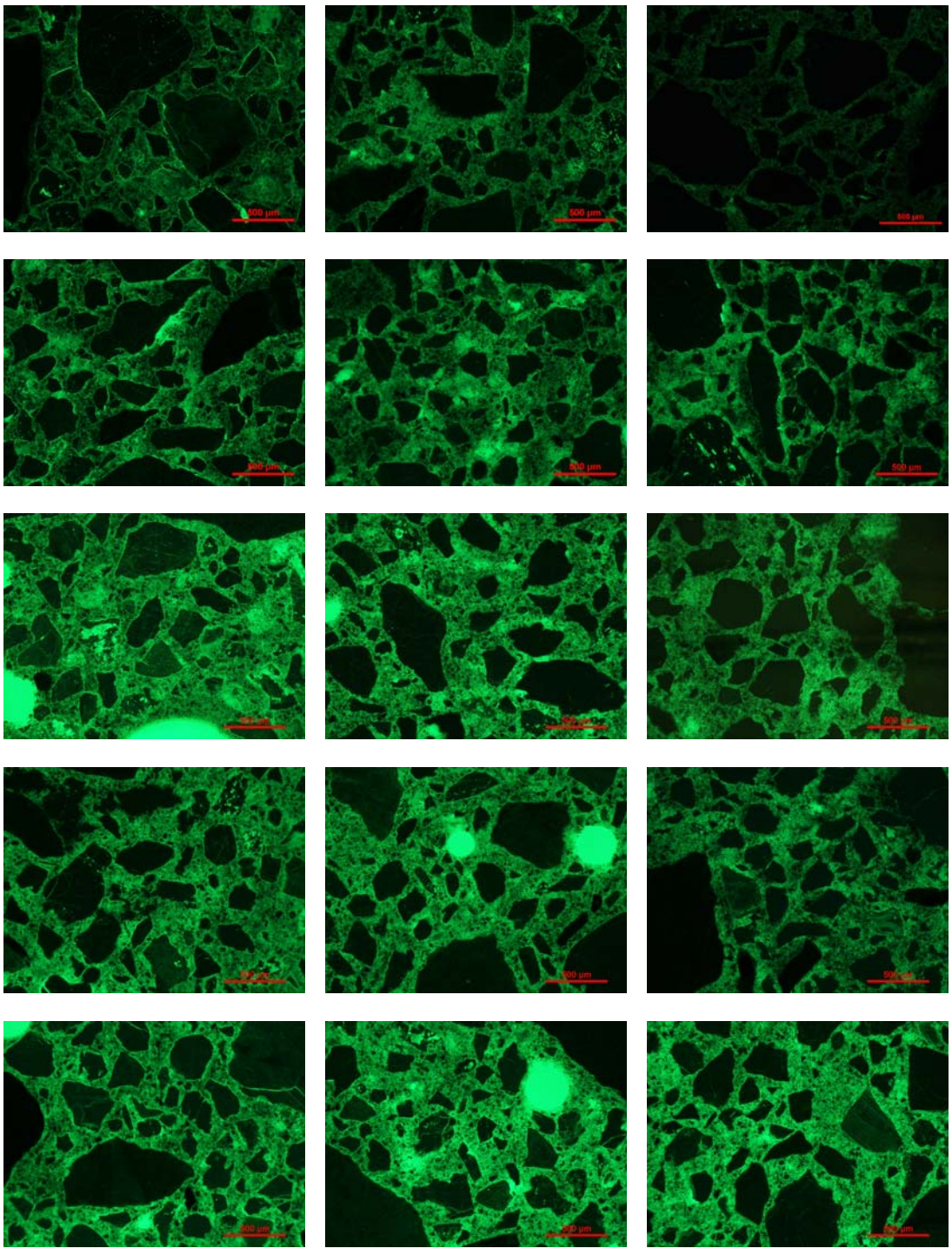

Figure 6.7 : Thin section photos of the samples C1, C2, C3, C4 and C5 (under UV light on the 1st, 3rd and 7th days after casting) (w/c ratio increase↓, time→)

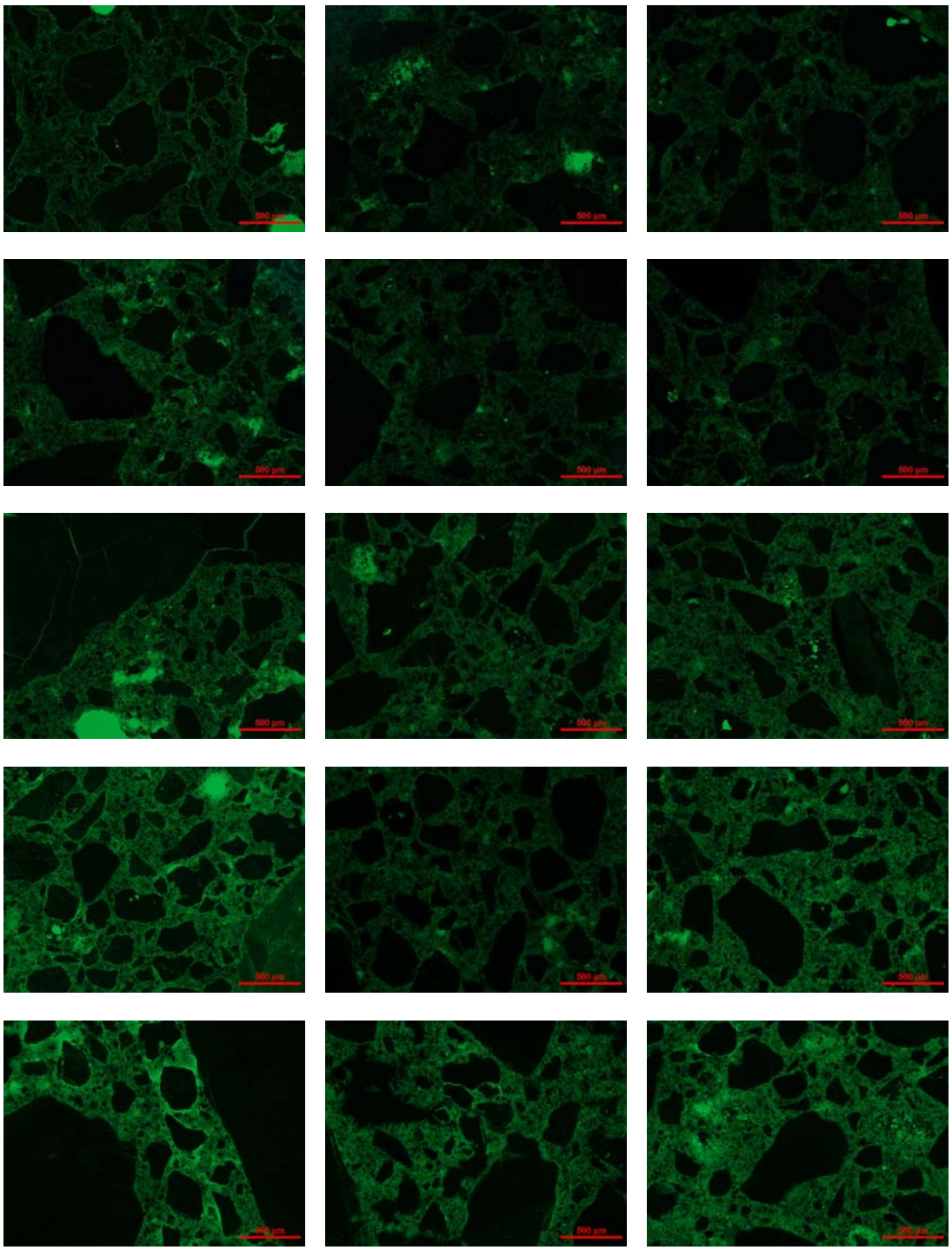

Figure 6.8 : Thin section photos of the samples SF1, SF2, SF3, SF4 and SF5 (under UV light on the 1st, 3rd and 7th days after casting) (w/c ratio increase↓, time→)

The luminosity increase with the increasing w/c ratio for both sets, with cement only and with cement and mineral additives. It is also obtained that samples with the mineral additives have less luminosity than samples with only cement, which indicates the filler effect of fly ash and microsilica. Another result, which can be obtained from the measurements, is the decreasing luminosity in time. 7 days samples are darker than the very early age samples, which shows the effect of hydration on capillary porosity dramatically.

On the other hand it is denotable, that this technique tells only the approximate amount of the capillary pore system, not the connectivity of every single capillary pore. Capillary pores are considered to have a size ranging from hundreds of micrometers down to tens of nanometers, which means that at one point on the thin section may exist much more capillary pores than the considered number. But the 50x magnification allows researchers also to see increased capillary pores around aggregates, which are obviously a sign for the existence of weak interfacial transition zones. When these interfacial transiton zones intersect on the section, it gives also an idea to researchers about the connectivity, which should be considered prominently.

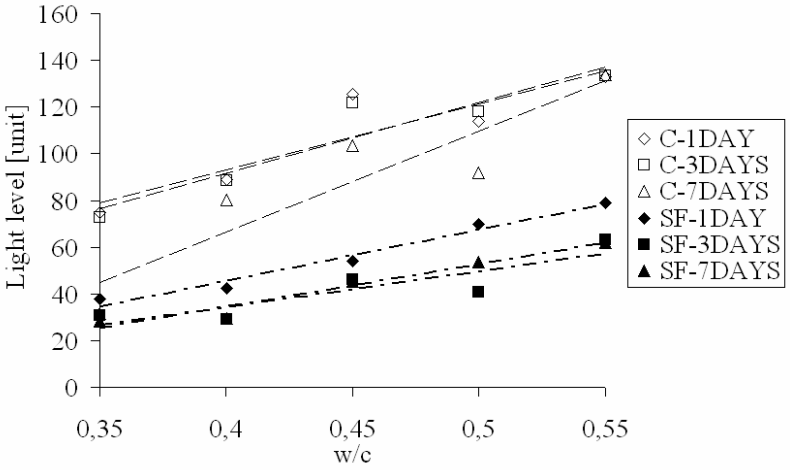

Figure 6.9 : w/c vs. light level

From the adiabatic heat development test, the following results can be obtained as shown below in **Figure 6.10**. The rate of hydration increase significantly, with the increase of w/c ratio. Another result is that the concrete with mineral additives produced much energy than the concrete without mineral additives and with the same w/c ratio at the same time interval.

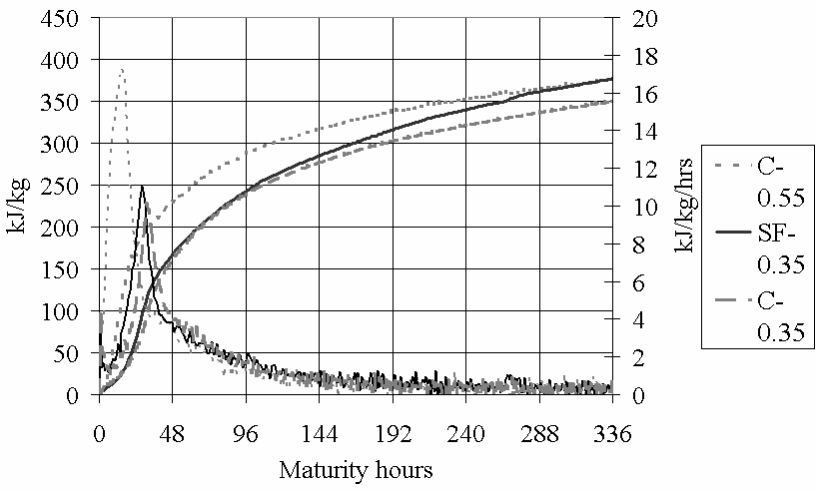

Figure 6.10 : Adiabatic heat development of concrete samples

When the **Figures 6.9** and **6.10** are considered together, they seem contradicting each other. For example, C-0.55 is hydrated rapidly in comparison to C-0.35, which means C-0.55 should have less volume for capillary pores than C-0.35, because of the formation of hydration products. On the other hand the light level in **Figure 6.9** shows that the luminosity for C-0.55 is greater than C-0.35, which means a greater capillary pore volume. This case can be explained with the loose packing of cement particles in higher w/c ratios, so the hydration products cannot fill the space between the cement particles, and capillary pores remain or vice versa, hydration products form easily, because there is enough space to settle for them. This relationship shows the importance of the gel to space ratio in cement paste. The amount of total hydration products does not affect the luminosity of specimens, in other words gel to space ratio determines the luminosity. This statement supports, what **Hu and Stroeven (2004)** stated before that in the fresh state of particle packing, the wall-effect causes of a reduction in the cement particle density, which implies a more porous zone than the bulk paste. It yields the conclusion, the capillary pore volume is the result of that porous zone. Moreover, after some time the light level decreases significantly, which proves the effect of hydration on capillary porosity.

The temperature developments of concretes are parallel to the results in the chart above in **Figure 6.10**. The concrete sample with high w/c ratio exceeded 35°C, other samples exceeded only 30°C as shown below in **Figure 6.11**. The graphic below shows, how an important role the ambient temperature plays during the testing. A small amount of increase in the ambient temperature delays the cooling of the concrete sample.

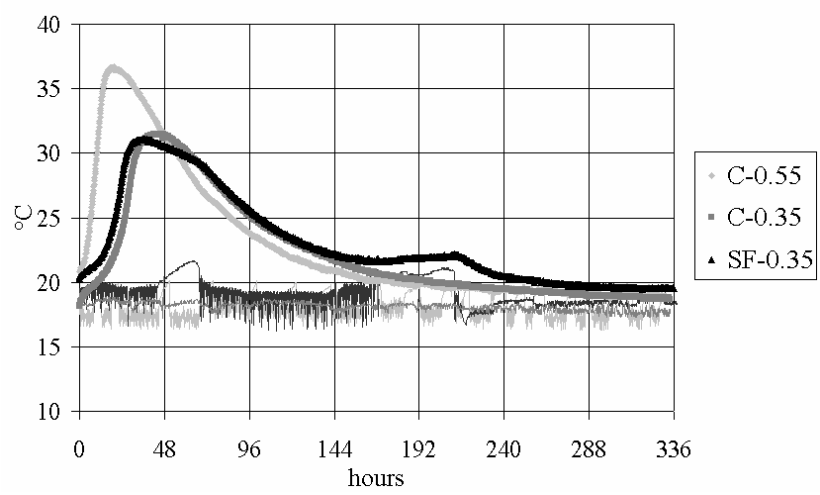

Figure 6.11 : Concrete and ambient temperatures during adiabatic heat development

From the chloride diffusion test results obtained from the non-linear regression analysis on hardening concrete specimens, the effective chloride transport coefficient, De, and the penetration parameter, K_{Cr} decrease with time as shown in **Figure 6.12** and **Figure 6.13**. , which is a reasonable result, because of the formation of hydration products with time.

Another result is the effect of water to cement ratio on the effective chloride transport coefficient and the penetration parameter. With increasing water to cement ratio De and K_{Cr} values increase as shown in **Figure 6.12** and **Figure 6.13**.

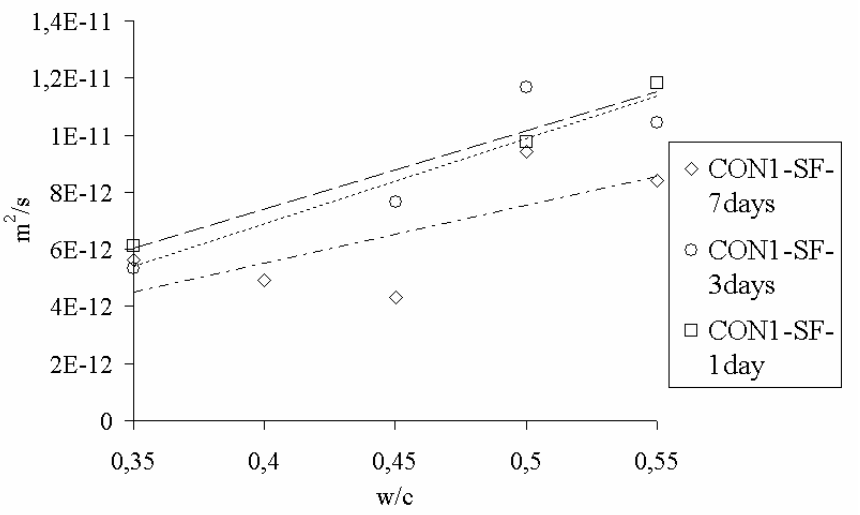

Figure 6.12 : w/c vs. effective chloride transport coefficient, De

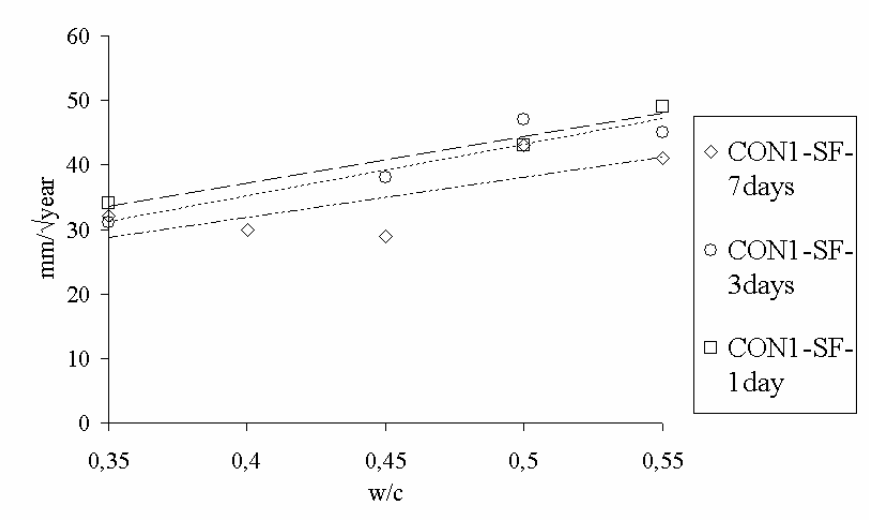

Figure 6.13 : w/c vs. penetration parameter, K_{Cr}

To compare gel to space ratio results with the compressive strength, light level and diffusion coefficient results the following **Table 6.2** is prepared. Some compressive strength results are excluded in curve fitting process, which are shown with asterix.

Table 6.2: Compressive strength, light level and and diffusion coefficient results corresponding to gel/space ratio values of C and SF pastes

C				SF			
Gel to space ratio	Compressive strength [MPa]	Light level [unit]	Diffusion coefficient [m^2/s]	Gel to space ratio	Compressive strength [MPa]	Light level [unit]	Diffusion coefficient [m^2/s]
0,474	4,6*	74,9	-	0,489	3,0*	38,0	6,13E-12
0,585	36,7	72,7	-	0,606	31,8	30,7	5,33E-12
0,663	54,1	31,6	-	0,682	42,8	28,4	5,62E-12
0,485	6,4*	89,1	-	0,492	15,7	42,2	-
0,536	33,2	88,4	-	0,560	32,8	29,1	-
0,625	47,8	80,3	-	0,646	47,2	29,5	4,9E-12
0,400	10,9	125,5	-	0,425	12,2	54,1	-
0,481	29,0	121,6	-	0,514	27,9	46,1	7,65E-12
0,576	41,4	103,5	-	0,602	40,1	45,2	4,33E-12
0,376	14,8	114,0	-	0,401	7,6	69,8	9,76E-12
0,454	29,4	118,0	-	0,485	17,5	40,9	1,17E-11
0,531	39,0	91,9	-	0,561	25,6	53,7	9,41E-12
0,347	9,6	132,9	-	0,373	6,5	79,0	1,18E-11
0,419	18,1	133,5	-	0,453	15,9	63,1	1,04E-11
0,492	26,5	133,9	-	0,522	22,7	62,1	8,42E-12

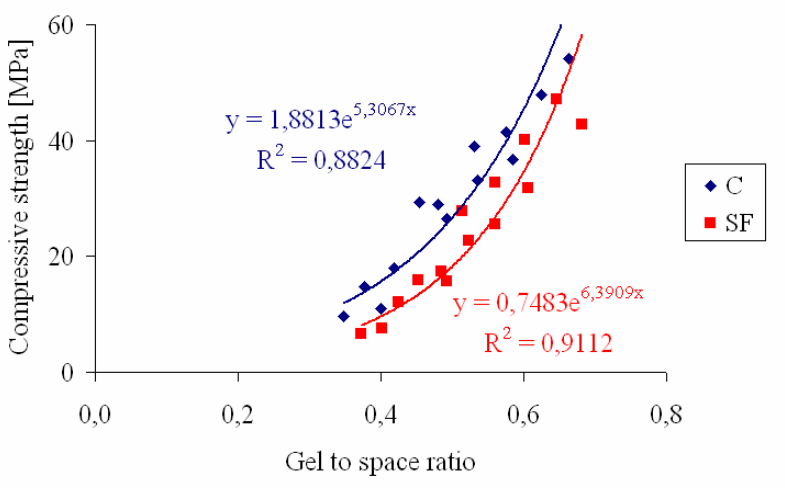

Figure 6.14 : Gel to space ratio vs. compressive strength

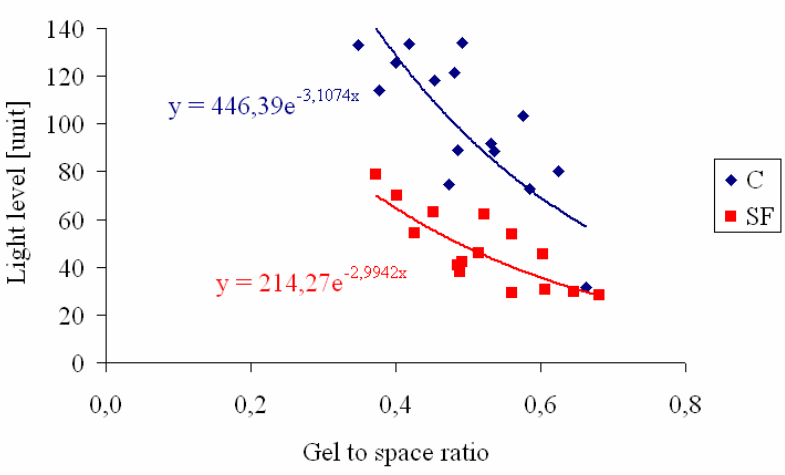

Figure 6.15 : Gel to space ratio vs. light level

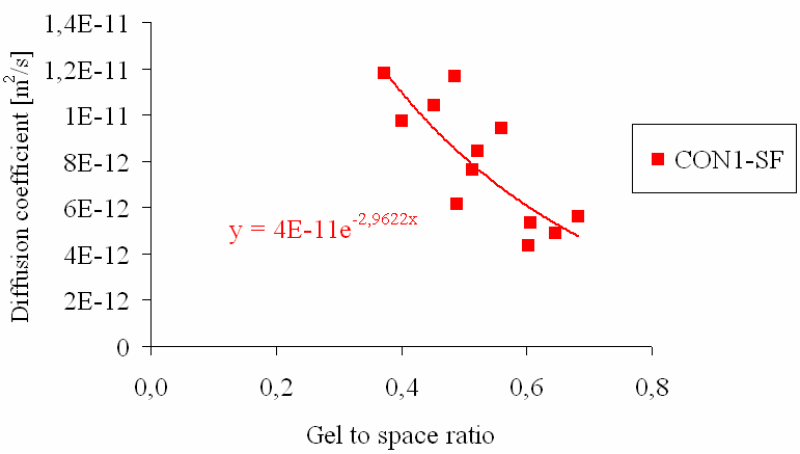

Figure 6.16 : Gel to space ratio vs. diffusion coefficient in hardening concrete

Figure 6.14 shows the strong relationship of gel/space ratio with compressive strength. Early-age strength increases with the increase of gel/space ratio. At the same value of gel/space ratio for both curves, C pastes have higher strength values than SF pastes at the early-age. Another result is SF pastes have higher gel/space ratio than C pastes for the same strength values.

Light level decreases for both C and SF pastes, with the increase of gel/space ratio as shown in **Figure 6.15**. At the same value of gel/space ratio for both curves, C pastes have more luminosity than SF pastes, which indicates the filler effect of fly ash and microsilica and the pozzolanic effect of mineral admixtures by joining the hydration process. Another result is SF pastes are filled with more gel than C pastes for the same light levels

Figure 6.16 shows that the increase of gel/space ratio yields a decrement at the effective chloride diffusion coefficient. This statement is parallel to the paragraph above, because high gel/space ratio values prevent the capillary transport in the gel.

As mentioned in previous paragraph **6.1** compressive strength decreases with increasing w/c ratio. It is shown again in **Figure 6.17**, that this statement is also true for hardened concrete samples.

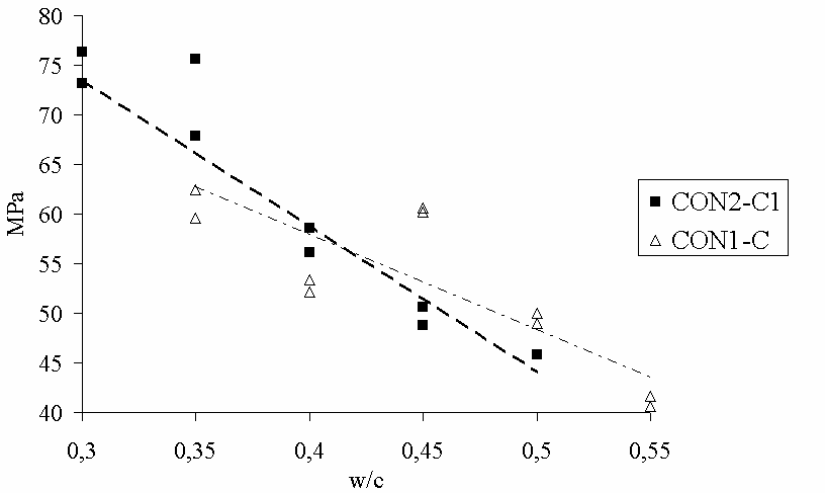

Figure 6.17 : w/c vs. compressive strength in hardened concrete

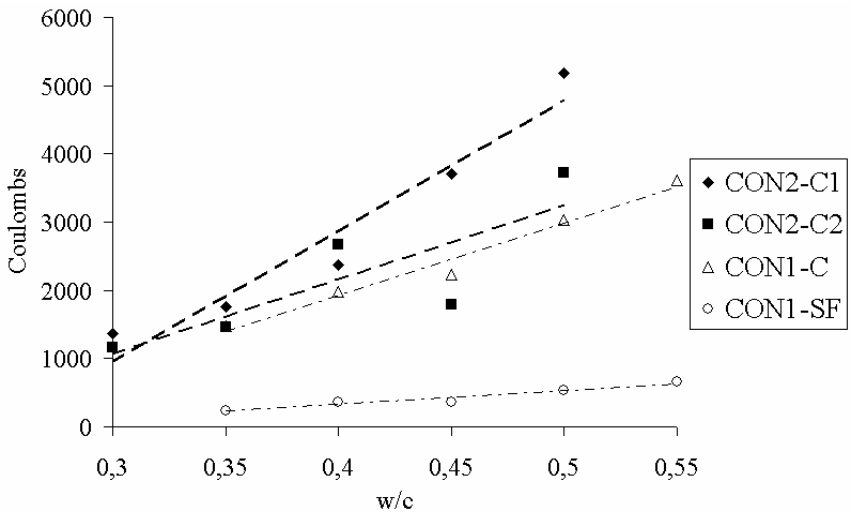

Figure 6.18 : w/c vs. charge passed in hardened concrete

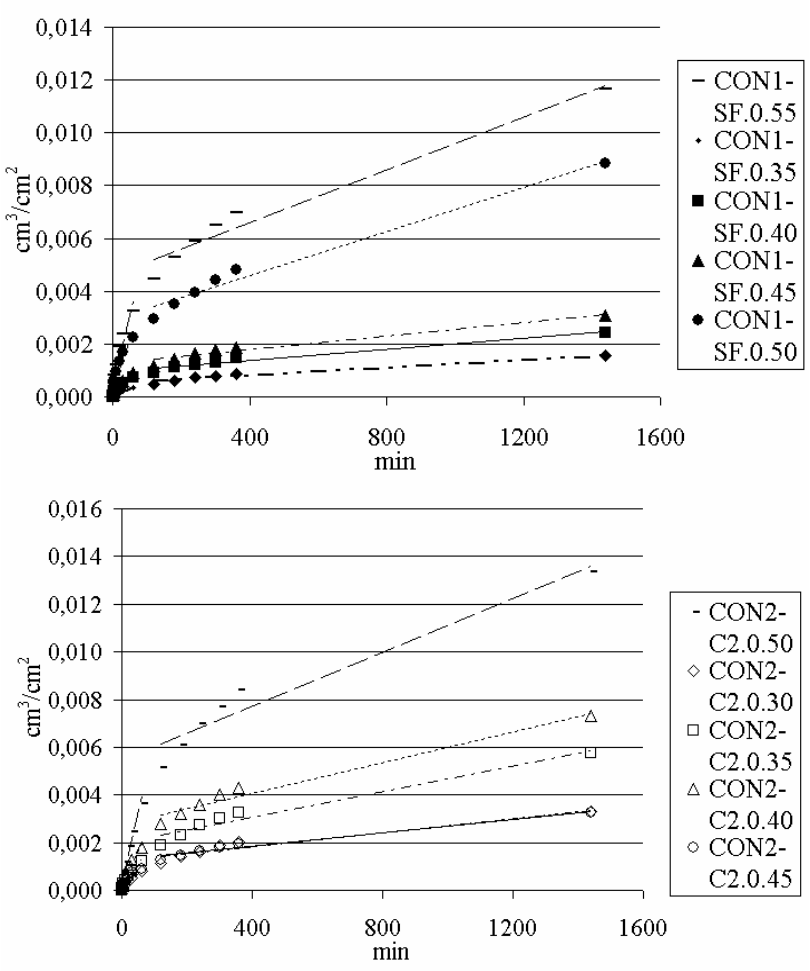

Figure 6.19 : Time vs. amount of water absorbed by capillary sorption

It has been told in previous chapter that during rapid chloride permeability test some unwanted interruptions have occured and no clear trend was obtained for the chloride permeability of concrete. But for the hardened conrete samples some results are obtained, which are shown in **Figure 6.18**. The adjusted charge passed through the specimens increase with the increasing of w/c ratio. Secondly, concrete specimens with mineral additives performed significantly, so that the passed charge values of cement concretes are about six times greater than those mineral added concrete specimens.

Another test, which is applied to hardened concrete samples is the capillary water absorption test according to **ASTM C 1585 (2004)**. Test results show that the w/c ratio affects the amount of water absorbed by capillary sorption dramatically. The increase of w/c ratio, increases the amount of water absorbed by capillary sorption. In addition to this, the absorption rate is variable. For a linear curve fitting for the obtained data, the absorption values are splitted into two parts according to the guidance of the standard, so initial and secondary absorption rates are indicated as shown in **Figure 6.19**. and the change in the absorption rate depending on w/c ratio is shown in **Figure 6.20**.

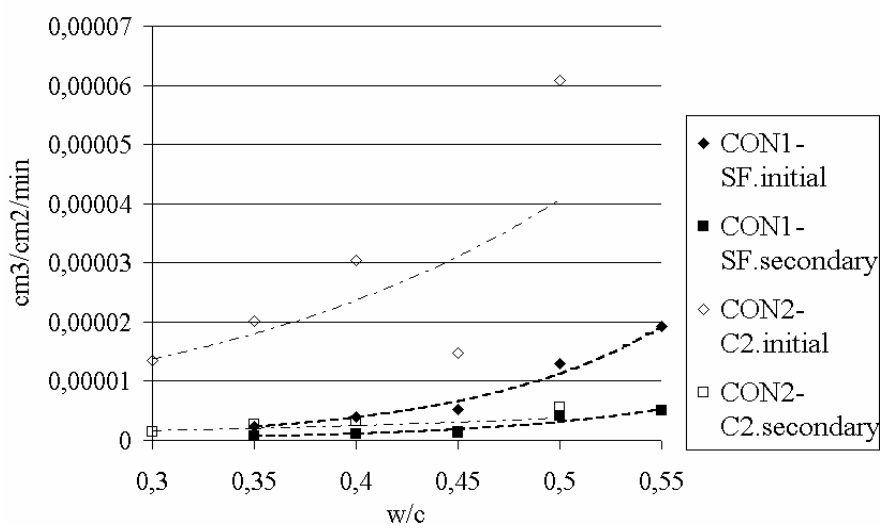

Figure 6.20 : w/c vs. capillary water absorption rate in hardened concrete

On **Table 6.3** are shown compressive strength and corresponding capillary water absorption rates. It is obtained from the **Figure 6.21** and **Figure 6.22** that the compressive strength decreases with the increase of both capillary water absorption rates, inital and secondary.

Table 6.3: Compressive strength and corresponding water absorption rate results

CON2-C2			CON1-SF		
Strength	initial capillary water absorption rate	secondary capillary water absorption rate	Strength	initial capillary water absorption rate	secondary capillary water absorption rate
[MPa]	10^{-5} [$cm^3/cm^2/min$]		[MPa]	10^{-5} [$cm^3/cm^2/min$]	
74,7	1,34	0,15	61,0	0,24	0,07
71,8	2,01	0,27	52,8	0,39	0,10
57,3	3,03	0,32	60,4	0,52	0,13
49,7	1,48*	0,14*	49,5	1,30	0,42
45,8	6,09	0,56	41,2	1,93	0,50

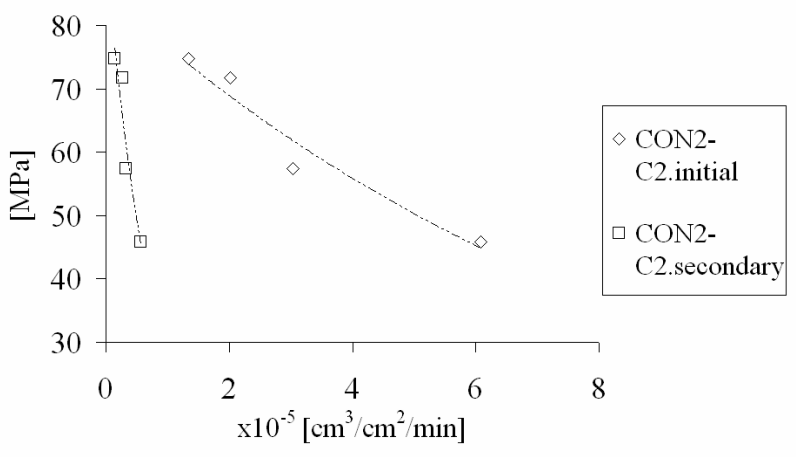

Figure 6.21 : Compressive strength vs. capillary water absorption rate in CON2-C2 concrete

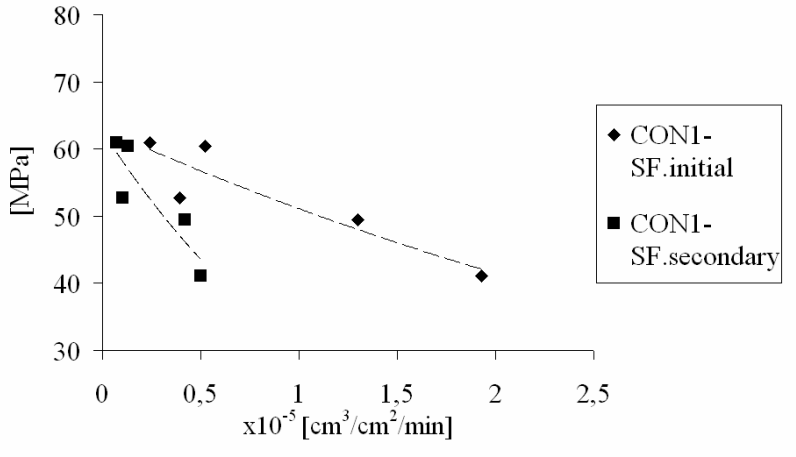

Figure 6.22 : Compressive strength vs. capillary water absorption rate in CON1-SF concrete

Figure 6.23 shows the strong relationship of gel/space ratio with capillary water absorption rate in hardened concrete. Absorption rate decreases with the increase of gel/space ratio.

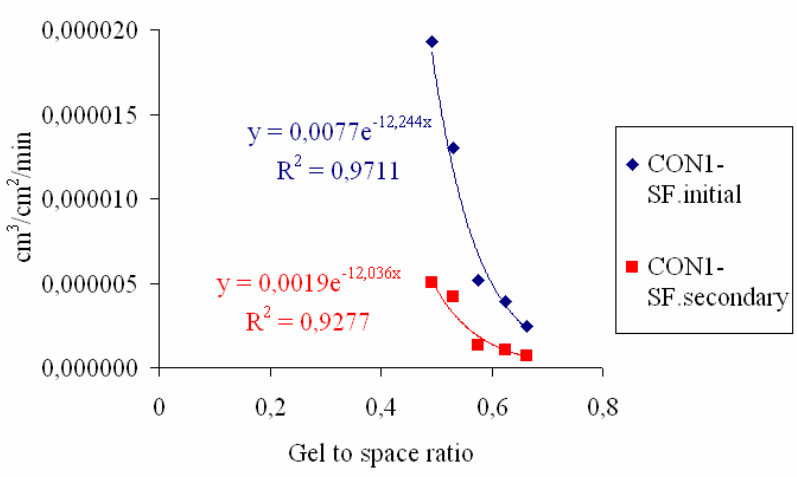

Figure 6.23 : Gel to space ratio vs. capillary water absorption rate in hardened concrete

As explained in paragraph **3.2** in an air void analysis, the entrapped and entrained air voids are investigated, because capillary pores are submicroscopic and cannot be measured via microscopic methods. But the need to know the pore structure of concrete completely, the air void analysis became an important tool for researchers.

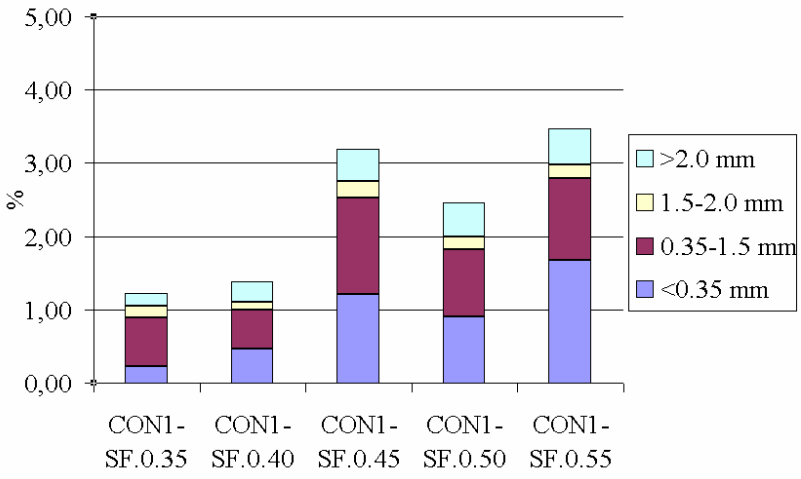

Figure 6.24 : Total air content results for CON1-SF set

The results of the analysis indicate that total air content increases with increasing w/c ratio as shown in **Figure 6.24**. This increment trend is not only at the total air content value, but also in each size interval classified as shown below in **Figure 6.25**. Another obtained result is that the average total air content of CON2-C2 is greater than CON1-SF, which indicates that the addition of mineral additives reduces the total air content. On the other hand, it is denotable that the above reached result of an air content increment depending on w/c ratio is not obtained at the CON2-C2 concrete as shown in **Figure 6.26** and **Figure 6.27**.

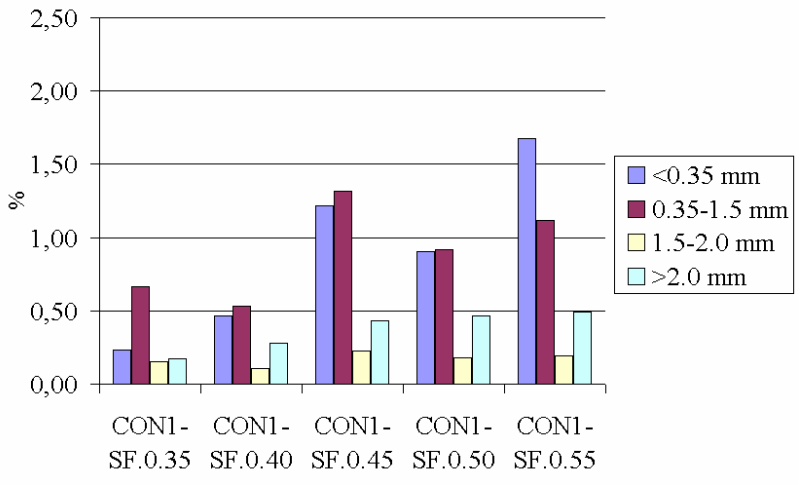

Figure 6.25 : Air void size distribution for CON1-SF set

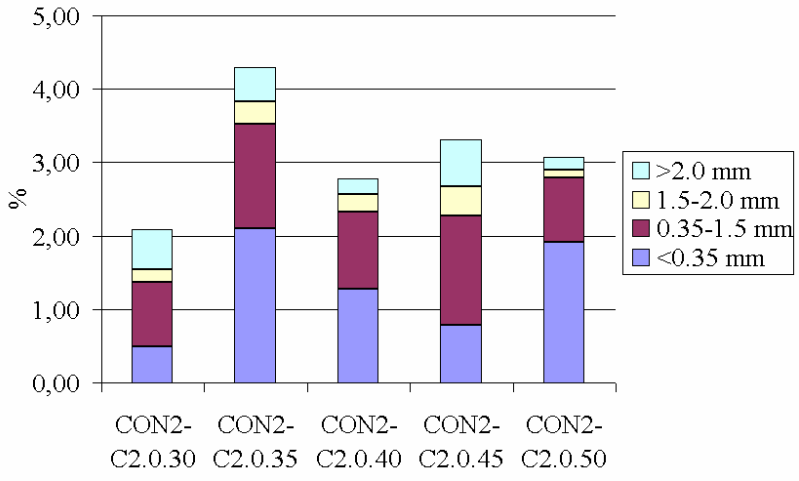

Figure 6.26 : Total air content results for CON2-C2 set

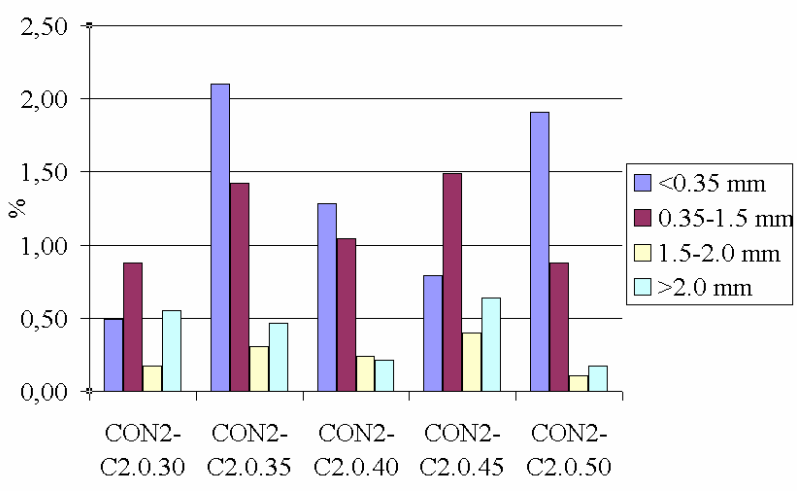

Figure 6.27 : Air void size distribution for CON2-C2 set

7. CONCLUSION

Concrete may be considered as the most complex composite material, composed of solid and liquid phases and pores with high degree of heterogenity. One of the elements of this complex structure is the capillary pore structure, which is affected by many physical and chemical processes, so that, these processes influence the durability based performance of concrete significantly.

The solid constituent materials' fineness and particle size distribution affects the pore structure, for example the volume of smaller pores is higher in finer cement. Secondly, the packing structure of solid constituents have incredible effects to the pore volume. The pore volume decreases with denser packing of cement particles. Thirdly, high w/c ratios increase the volume of larger pores. At this work, the effect of w/c ratio was very obvious especially in light intensity analysis and capillary water absorption test. The capillary pore space volume is proportional to the w/c ratio.

Hydration is the most important chemical process affecting the capillary porosity. During hydration, hydration products fill the available space in the pore structure gradually, so the connected capillary pore structure depercolates and become disconnected.

Finally, exposure conditions are very effective on the durability based performance of concrete structures. Harsh climatic conditions may deteriorate concrete structures rapidly. Therefore engineers' responsibilities expanded from improving structures mechanical qualifications to providing structures durability performance.

REFERENCES

Abell, A.B., Willis, K.L. and Lange, D.A., 1999. Mercury intrusion porosimetry and image analysis of cement-based materials, *Journal of Colloid and Interface Science, 211***,** 39-44.

Akyüz, S., Akkaya, Y., Yazan, H.O. and Taşdemir, M.A., in press. Damage mechanics based modelling of the relation between capillary pores and compressive strength of concrete, *Fracture Mechanics of Concrete and Concrete Structures Conference,* Catania, Italy.

ASTM C 457, 1998. Standard test method for microscopical determination of parameters of the air-viod system in hardened concrete, *American Society for Testing and Materials,* United States.

ASTM C 1202, 2005. Standard test method for electrical indication of concrete's ability to resist chloride ion penetration, *American Society for Testing and Materials,* United States.

ASTM C 1585, 2004. Standard test method for measurement of rate of absorption of water by hydraulic cement concretes, *American Society for Testing and Materials,* United States.

Bentz, D.P., 1997. Three-dimensional computer simulation of portland cement hydration and microstructure development, *Journal of American Ceramic Society,* **80,** 3-21.

Bentz, D.P. and Garboczi, E.J., 1999. in *Engineering and Transport Properties of the Interfacial Transition Zone in Cementitous Composites,* pp. 349, Eds. Alexander, M.G., Arligue, G., Ballivy, G., Bentur, A. & Marchand, J., RILEM Publications SARL. ENS, Cachan.

Diamond, S., 2000. Review, Mercury porosimetry: An inappropriate method for the measurement of pore size distributions in cement-based materials, *Cement and Concrete Research,* **30,** 1517-1525.

DS 423.40, 2002. Testing of concrete - Hardened concrete - Production of fluorescence impregnated thin sections, *Danish standards association,* Denmark.

DS 423.41, 2002. Testing of concrete - Hardened concrete – Internal stability, *Danish standards association,* Denmark.

DS 423.42, 2002. Testing of concrete - Hardened concrete – Concrete composition, *Danish standards association,* Denmark.

DS 423.43, 2002. Testing of concrete - Hardened concrete – Paste homogeneity, *Danish standards association,* Denmark.

DS 423.44, 2002. Testing of concrete - Hardened concrete – Paste cracks and bond cracks, *Danish standards association,* Denmark.

DS 423.45, 2002. Testing of concrete - Hardened concrete – Degree of compaction, *Danish standards association,* Denmark.

DTI, 2003a. Adiabatic heat calculation sheet Ver. 1.0, *Danish technological institute,* Denmark.

DTI, 2003b. 4C Temp&Stress 2.10, rel.7, *Danish technological institute,* Denmark.

Feldman, R.F. and Sereda, P.J., 1968. A model for hydrated portland cement paste as deduced from sorption length cahange and mechanical properties, *Materials and Structures,* **1,** 509.

Halamickova, P., Detwiler, R.J., Bentz, D.P. and Garboczi, E.J., 1995. Water permeability and chloride ion diffusion in portland cement mortars: Relationship to sand content and critical pore diameter, *Cement and Concrete Research,* **25,** 790-802.

Hu, J., 2004. Porosity of concrete, morphological study of model concrete, *PhD Thesis,* TU Delft, Delft.

Hu, J. and Stroeven, P., 2004. Properties of the interfacial transition zone in model concrete, *Interface Science,* **12,** 389-397.

Jaiswal S.S., Picka J.D., Igusa T., Karr A.F., Shah, S.P., Ankenman, B.E. and Styer, P., 1998. Experimental studies of the chloride permeability of concrete*, National Institute of Statistical Sciences Technical Report,* **87,** Research Triangle Park, NC.

Kurtis, K., 2007. Kimberly Kurtis. , *http://www.ce.gatech.edu/~kk92/concrete.html/hcp.pdf*.

Lam, L., Wong, Y.L. and Poon, C.S., 2000. Degree of hydration and gel/space ratio of high-volume fly ash/cement systems, *Cement and Concrete Research,* **30,** 747-756.

Laugesen, P., 1993. Effective w/c ratio of cement paste in concrete, *Proc. 4th Euroseminar on Microscopy Applied to Building Materials,* Wisby, Sweden.

Mindess, S. and Young, J.F., 1981. Concrete. Prentice-Hall, Inc., Englewood Cliffs, NJ.

Nilsson L.O., Poulsen E., Sandberg P., Sørensen H.E. and Klinghoffer O., 1996. HETEK, Chloride penetration into concrete, State-of-the-Art, Transport processes, corrosion inititation, test methods and prediction models*, Danish Road Directorate,* **Report no.53**.

NT BUILD 388, 1992. Concrete: Heat development, *NORDTEST,* Finland.

NT BUILD 443, 1995. Concrete, Hardened: Accelerated chloride penetration, *NORDTEST,* Finland.

PCA, 2007. Portland Cement Association, Concrete Technology and Construction: Durability, *http://www.cement.org/tech/cct_durability.asp*.

Powers, T.C. and Brownyard, T.L., 1948. Studies of the physical properties of hardened cement paste, *Research Laboratories of the Portland Cement Association Bulletin*, **22**, Chicago.

Ramachandran, V.S. and Beaudoin, J.J., 2001. Handbook of analytical techniques in concrete science and technology, Noyes Publications & William Andrew Publishing LLC, New York.

Scrivener, K.L., 1999. Characterisation of the ITZ and its quantification by test methods, In *Engineering and Transport Properties of the Interfacial Transition Zone in Cementitous Composites,* pp. 3-15, Ed. Alexander, M.G., RILEM Publications SARL. ENS, Cachan.

Scrivener, K.L., Crumbie A.K. and Laugesen, P., 2004. The interfacial transition zone (ITZ) between cement paste and aggregate in concrete, *Interface Science,* **12,** 411-421.

Stanish K.D., Hooton R.D. and Thomas M.D.A., 1997. Testing the chloride penetration resistance of concrete: A literature review*, Prediction of chloride penetration in concrete,* **FHWA Contract DTFH61-97-R-00022**.

Stark, J., Möser, B. and Eckart, A., 2001. Neue Ansätze zur Zementhydratation, *ZKG International,* pp.52, Germany.

TS EN 12390-3, 2003. Testing hardened concrete – Part:3 Compressive strength of test specimens, *Türk Standartları Enstitüsü,* Ankara.

Yang, T., 2006. AFM Study of the interactions between moisture and the surface of cementitious materials, *PhD Thesis,* ETH, Zurich.

Zimbelmann, R., 1985. A contribution to the problem of cement-aggregate bond, *Cement and Concrete Research,* **15,** 801-808.

CURRICULUM VITAE

Hüseyin Oytun YAZAN was born in Istanbul in 1982. He is graduated from German High School in 2001. He received his B.Sc. degree in Civil Engineering from Istanbul Technical University in 2005. He started studying for his master's degree in 2005 in Structural Engineering Program at Istanbul Technical University.